A Review of Integrated On-Board EV Battery Chargers: Advanced Topologies, Recent Developments and Optimal Selection of FSCW Slot/Pole Combination

MOHAMED Y. METWLY[1,3]**, MAHMOUD S. ABDEL-MAJEED**[1,3]**,**
AYMAN S. ABDEL-KHALIK[2]**, (Senior Member, IEEE),**
RAGI A. HAMDY[2]**, (Senior Member, IEEE), MOSTAFA S. HAMAD**[3]**, (Senior Member, IEEE),**
AND SHEHAB AHMED[4]**, (Senior Member, IEEE)**

[1]Smart-CI Center, Alexandria University, Alexandria 21544, Egypt
[2]Department of Electrical Engineering, Alexandria University, Alexandria 21544, Egypt
[3]Department of Electrical and Control Engineering, Arab Academy for Science, Technology and Maritime Transport, Alexandria 1029, Egypt
[4]CEMSE Division, King Abdullah University of Science and Technology, Thuwal 23955, Saudi Arabia

Corresponding author: Ayman S. Abdel-Khalik (ayman.abdel-khalik@alexu.edu.eg)

ABSTRACT Integrated on-board battery chargers (OBCs) have been recently introduced as an optimal/elegant solution to increase electric vehicle (EV) market penetration as well as minimize overall EV cost. Unlike conventional off-board and on-board battery chargers, integrated OBCs exploit the existing propulsion equipment for battery charging without extra bulky components and/or dedicated infrastructure. OBCs are broadly categorized into three-phase and single-phase types with unidirectional or bidirectional power flow. This paper starts with surveying the main topologies introduced in the recent literature employing either induction or permanent magnet motors to realize fully integrated slow (single-phase) and fast (three-phase) on-board EV battery charging systems, with emphasis on topologies that entail no or minimum hardware reconfiguration. Although, permanent magnet (PM) motors with conventional double-layer distributed winding layouts have been deployed in most commercial EV motors, the non-overlapped fractional slot concentrated winding (FSCW) has been the prevailing choice in the most recent permanent magnet motor designs due to its outstanding operational merits. Hence, a thorough investigation of the impact different FSCW stator winding designs have on machine performance under the charging process is presented in this paper. To this end, the induced magnet losses, which represent a challenging demerit of the FSCW, have been used to compare different topologies under both propulsion and charging operation modes. Based on the introduced comparative study, the optimal slot/pole combinations that correspond to the best compromise under both operational modes have been highlighted.

INDEX TERMS Integrated chargers, on-board battery chargers (OBCs), multiphase machines, fractional slot concentrated winding (FSCW), battery charging, optimal slot/pole combinations, reviews.

I. INTRODUCTION

Automotive market analysis shows that the market share of electric vehicles (EVs) will be about 30% by 2030 [1]. Battery technology has a great effect on the expansion of EVs. The cost, weight, charging time and lifetime

The associate editor coordinating the review of this manuscript and approving it for publication was Atif Iqbal.

of the EV battery constitute vital challenges for commercialization. In addition to numerous electrochemistry and material challenges, the performance of battery modules is affected by module design/packaging as well as electrical charging and discharging characteristics [2], [3]. There is significant correlation between charging time, lifetime of the battery and the characteristics of the employed battery charger [4].

EV battery chargers can be broadly classified into off-board and on-board configurations with unidirectional or bidirectional power flow capability [5]. Unidirectional charging reduces hardware requirements and simplifies interconnection with the grid. Whereas, bidirectional charging permits battery power injection back to the grid. Off-board chargers are installed in dedicated charging stations which are designed to offer higher power transfer capabilities, albeit, at a high infrastructure cost. Numerous off-board charger topologies and control techniques have been introduced in the available literature [5]. On the other hand, vehicle on-board charging systems can be directly connected to single-phase or three-phase mains, which off-loads infrastructure cost. However, power transfer capability is typically limited due to several constraints/tradeoffs such as cost, volume, and weight of the vehicle [6]. Various topologies and control schemes of on-board chargers have been presented in [7]. Battery chargers are classified based on power level and charging time in Table 1 [5].

In order to overcome the limitations of on-board battery chargers (OBCs) while preserving their advantages, the so-called integrated OBCs exploit existing propulsion circuit components, the electric motor and the inverter, for battery charging instead of a separate charging circuit with bulky add-on inductors [8]. The motor windings are used as filter inductances and/or as galvanic isolation. Whereas, the propulsion inverter is used as a bidirectional DC/AC converter. This technology has recently emerged as an interesting optimal compromise between on-board and off-board battery chargers. The effectiveness of this technique entails some technical requirements, namely, limited/no winding reconfiguration and zero average torque and torque ripple production during the charging process. Achieving these desirable features will highly depend on the motor type, number of phases, and employed power converter [9].

The electric motor types utilized in EVs include induction motors (IMs), permanent magnet (PM) machines, and switched-reluctance motors (SRM) [10]. According to the analysis of battery electric vehicles (BEVs) introduced in [11], the PMSM is the most commonly used type in current BEVs. Nevertheless, most integrated onboard chargers in the available literature were based on IMs equipped with conventional distributed windings. The advantages of IMs include low cost, robustness, reliability, and low maintenance requirement [12]. On the other hand, PMSMs have the highest efficiency among all other EV drivelines [13]. SRMs are cost-effective and high performing, however, they have high torque ripple [14]. Continued interest in SRMs is mainly due to their high starting torque, wide-speed range and fault tolerance capabilities [15]. As an integrated OBC machine candidate, SRMs can produce zero average torque during charging, and their flexible energy flow control in EV applications is discussed in [16].

Although the three-phase machine is preferred for propulsion as evidenced by commercial deployments, additional considerations apply when considering an integrated OBC.

The three-phase machine requires extra nonintegrated components during the three-phase fast charging process to nullify the average torque production resulting from the flow of three-phase currents through the machine windings. Standard three-phase machines may be suitable for single-phase slow integrated OBC. The system introduced in [17] uses a synchronous machine with an excitation winding to avoid torque production during charging. However, hardware reconfiguration to allow transition between propulsion and charging mode is a necessity. Whereas, another solution that does not require any hardware reconfiguration is introduced in [18]. It employs four propulsion motors and has zero-torque production during fast charging mode, albeit at a high cost. As a result of these limitations, multiphase machines have gained significant attention because of the aforementioned demerits of their three-phase counterparts in integrated OBC applications.

Multiphase machines are advantageous over their three-phase counterparts in many ways. The converter rating per phase is reduced by splitting the power among more phases, while offering improved fault tolerance [19]. As far as EV drivetrains are concerned, multiphase machines can effectively ensure zero torque production during the charging period by exploiting the extra degrees of freedom of multiphase machines [20]. This enables viable realizations for integrated OBCs for EV applications. Despite the above-mentioned advantages, multiphase machines need a more complex inverter and controller. Additionally, the decoupling transformations utilized in multiphase systems are quite sophisticated when compared to their three-phase counterparts [21].

Early electric/hybrid vehicles employed high speed motors with mechanical gear transmission (drivetrain) to reduce motor speed and transmit motor power to the wheels. Recent designs, however, introduced low speed in-wheel-motor structures to avoid friction losses and maintain full torque capabilities [22]. However, the relation between the machine torque and size stands as the main challenge in order to achieve this vision [23]. In this context, the FSCW layout provides a powerful candidate when compared to a distributed winding (DW) in many of the aspects summarized in Table 2. The FSCW helps reduce end turn length, simplifies manufacturing and enables a slot fill factor approximately equal to 78%, especially when coupled with segmented stator structures [24]. These advantages result in a promising cost-effective solution. Recently, it has been proven that the design of PM machines with a multiphase fractional slot concentrated winding (FSCW) arrangement has a significant effect on flux-weakening and fault-tolerance capabilities [25].

PM machines equipped with a FSCW offer high torque density, high efficiency, low cogging torque, flux-weakening capability and fault tolerance. Nevertheless, the FSCW tends to produce non-uniform flux density distributions in the air gap. The non-synchronous space harmonics with relatively high magnitudes, including sub and super harmonics, induce eddy currents in the rotor core, which in-turn yield significant

TABLE 1. Battery charger classification in terms of power levels [5].

Power level types	Charger location	Typical use	Power level	Charging time
Level-1 120 Vac (US) 230 Vac (EU)	On-board 1-phase	Charging at home	1.4 kW (12A) 1.9 kW (20A)	4-11 hours 11-36 hours
Level-2 240 Vac (US) 400 Vac (EU)	On-board 1-or-3-phase	Charging at private or public outlets	4 kW (17A) 8 kW (32A)	1-4 hours 2-6 hours
Level-3 (208-600 Vac or Vdc)	Off-board 3-phase	Commercial or public	50 kW 100 kW	0.2-0.5 hours

TABLE 2. Diversity of distributed and concentrated winding layouts.

Winding Type	Distributed Winding	Concentrated Winding
Air gap flux quality	High quality flux distribution	Distorted flux distribution
Torque-producing flux component	Fundamental component	Higher order harmonic (The main slot harmonics)
Stator structure	Continuous laminated core	Continuous laminated or segmented structure
End turn	Long and overlapping	Short and non-overlapping

rotor losses [26]. Even though these losses are lower than the stator losses, their effect is crucial on machine performance [27]. The lack of ventilation in the rotor overheats the rotor magnets yielding inevitable thermal demagnetization [28]. Additionally, the interaction between these non-synchronous low order harmonics causes noise and undesired vibrations in the mechanical structure, the degree of which mainly depends on the adopted slot/pole combination [29]. The key components that affect the preferred slot/pole combinations are cogging torque, fill-factor, net radial forces and rotor losses [25]. In the literature, several interesting stator slot/pole combinations have shown promise in EV applications. Some of them are based on non-overlapped FSCW windings such as 12-slot/10-pole [30] and 18-slot/16-pole [31] combinations, while others are based on overlapped windings with a coil pitch of two, such as the 24-slot/10-pole [32] and 18-slot/10-pole [33] combinations. In the case of overlapped windings with a coil pitch of two, the air gap flux distribution is highly improved and the undesired slot harmonics are considerably suppressed.

The key objective of this paper is to first present an extensive up-to-date review of integrated OBCs for EV applications utilizing either three-phase or multiphase machines, which have been the topic of a significant body of recent literature. Integrated OBCs are reviewed with a further classification by type of power supply: slow single-phase charging, fast three-phase charging, and charging using a multiphase voltage source. Almost all indicated topologies support vehicle-to-grid (V2G) integration [34], [35]. The various types of chargers are investigated in terms of types of converters, technical challenges, advantages and limitations. Control techniques during charging mode (PQ control and voltage-oriented control) are also introduced. Due to the fact that PM machines equipped with a FSCW have proven themselves as a competitive option for EV traction, this paper

extends existing FSCW slot/pole combinations for EV applications with new six and nine-phase order multiphase FSCW arrangements. Furthermore, we present variations in rotor loss indices with respect to various FSCW slot/pole combinations for multiphase machines under both propulsion and charging modes, which represents another key contribution of this study/survey. Furthermore, non-overlapped FSCW slot/pole combinations are compared with overlapped windings ones (coil pitch of two) in terms of magneto motive force (MMF) distributions under different modes. Based on this comparative study, optimal slot/pole combination(s) emerge as a compromise between machine performance under both propulsion and charging modes.

II. INTEGRATED ON-BOARD CHARGER TOPOLOGIES

Integrated OBC chargers have been recently proposed to reduce the cost and weight of EVs. Integrated OBC challenges/drawbacks can be confined to average torque production during charging mode and hardware reconfiguration to switch between propulsion and charging modes. Considering that most commercial EVs are based on three-phase motors, various integrated chargers employing three-phase machines have been introduced in the literature [4], [36]. These topologies are simple and are preferably utilized while charging is achieved through single-phase mains. If three-phase charging is employed, the three-phase currents flowing in the stator windings will cause an average torque production, hence, a mechanical lock is required to prevent motor rotation. This solution considerably affects efficiency due to the high rotor copper and core losses. Moreover, mechanical wear is likely and audible noise is inevitably introduced. To mitigate this shortcoming, the application of multiphase machines has been adopted as they can successfully offer zero torque production during charging mode owing to their additional degrees of freedom. Various integrated onboard chargers
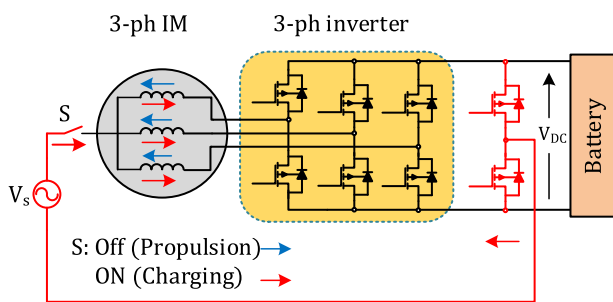
FIGURE 1. Thyristor-based integral battery charger.

FIGURE 2. Integrated charger based on two-motor drive.

based on multiphase drivetrains are considered in [37], [38]. Integrated chargers connected to a single-phase supply (slow charging), a three-phase grid (fast charging), or a multiphase voltage source (fast charging) are thoroughly reviewed in the following subsections.

A. SLOW SINGLE-PHASE CHARGING

Widespread availability of single-phase mains outlets mandates the need for single phase charging capability. However, single-phase charging can only offer slow charging levels. Moreover, single-phase charging corresponds to a pulsating charging power that undesirably affects battery lifetime [4], [37], [39]. This section will cover integrated OBC topologies based on both three-phase and multiphase machines connected to a single-phase supply during the charging process.

The single-phase integrated charger initially introduced in 1985 [40] is shown in Fig. 1. During propulsion, switch S is open, the machine is driven using a three-phase inverter. Charging mode is initiated by connecting a single-phase outlet between the machine star point and a fourth inverter leg when switch S is closed. During charging, the three inverter legs are controlled to ensure zero-sequence stator currents. This requirement for a fourth leg to allow for neutral current return is regarded as the main drawback of this technique, since the current rating of this additional leg is three times the other legs. On the other hand, both average and pulsating torques can be eliminated.

In the approach described in [41], the integrated charger consists of a bidirectional DC power source, two IMs, two voltage-fed inverters, and a control unit, as depicted in Fig. 2. This topology can be implemented using two different approaches either two separate IMs or a single motor with dual three-phase stator winding sets. During propulsion mode, power is transferred from the DC supply, battery, to the two motors sharing the total driving torque. During the charging process, the single-phase grid is attached to the neutral points of the two motors. The main advantages of this solution include zero average torque production during the charging process, no need for mechanical a differential during propulsion mode, and the ability to inject battery energy back to the grid. An improved solution for controlling such a system, that incorporates the same configuration, is discussed in [42],
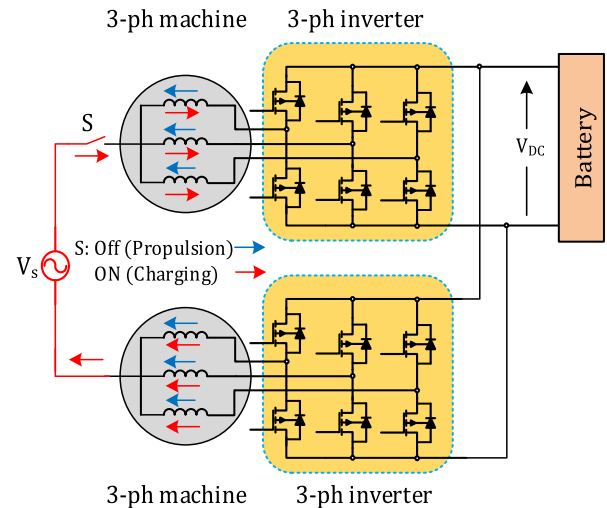
where an interleaving switching technique was introduced to effectively improve the efficiency and current waveforms concurrently. This way, the grid current ripple diminishes when compared to the phase current ripple due to the effective tripling of its ripple frequency. The main drawback of this topology is the pulsating nature of the battery charging power at the double line frequency since it is still based on a single-phase supply.

Another solution that incorporates a single-phase-based charger is depicted in Fig. 3 [43]. It employs powertrain elements, namely a three-phase induction motor and conventional three-phase inverter, in association with three additional relays K1, K2, and K3. These relays are utilized for reconfiguring the motor windings during various modes of operation. Under propulsion, K1 is closed, while K2 and K3 are open, resulting in a conventional three-phase propulsion system. The relays swap their opening and closing conditions during the charging mode (K2 and K3 are closed and K1 is open). During charging, the motor leakage inductances act as boost inductors. Two legs of the inverter, specifically switches S3-S6, are controlled using pulse width modulation (PWM) and operate as a boost converter. The battery voltage is selected to be of greater value than the grid peak voltage in order to ensure unity power factor operation can be achieved. The filter block, shown in Fig. 3, is used to minimize line current harmonic distortion. This solution underpins the V2G concept and is currently used in some commercial cars. The existence of the relays constitutes the main drawback of this topology because it may increase conduction losses.

A four motor-drive based integrated charger has been introduced in [44]. It consists of four induction motors (IMs), four three-phase inverters, a battery, and a transfer switch. The transfer switch allows the transition between the propulsion and charging modes (hardware reconfiguration is needed). Fig. 4 presents the equivalent charging scheme of this solution, where the single-phase source is connected to the neutral
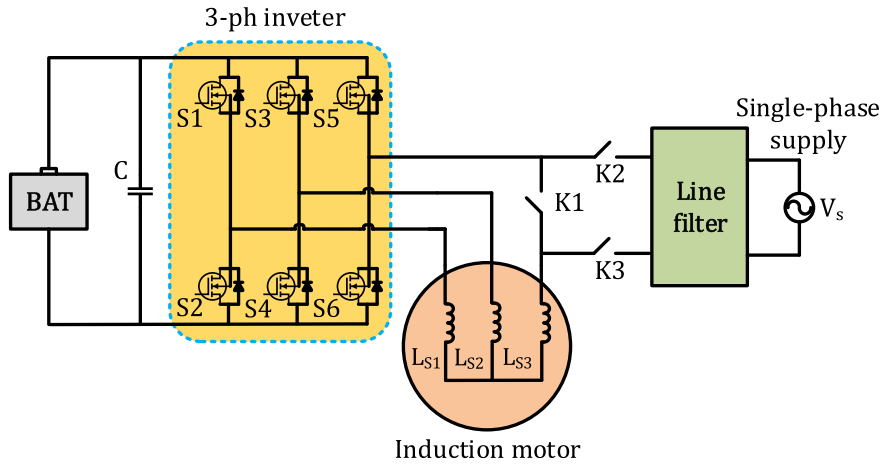
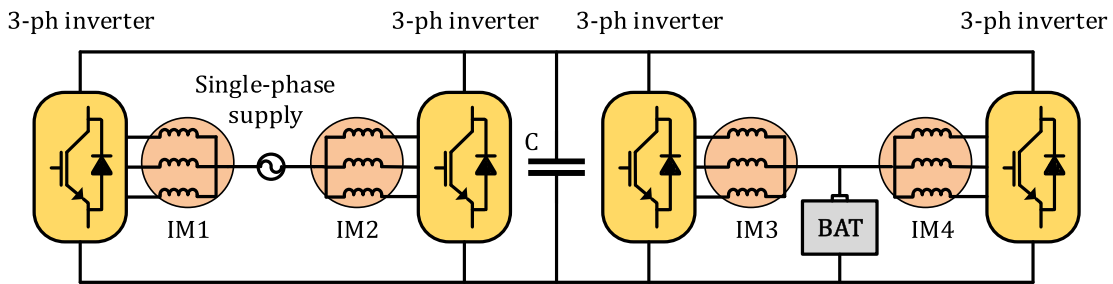**FIGURE 3.** Single-phase integrated charger based on IM-drive.

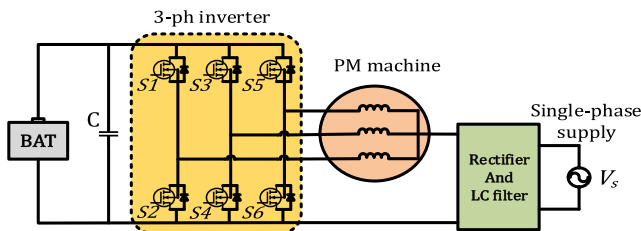**FIGURE 4.** Charging scheme of integrated four-wheel drive.

FIGURE 5. Single-phase integrated charger based on PM-drive.

points of motors IM1 and IM2; while the neutral points of the other two motors (IM3 and IM4) are connected to the battery. Motors 1 and 2 along with their allocated inverters are employed as a single-phase boost converter, unity power factor operation at the grid side can therefore be obtained. Motors 3 and 4 act as a part of DC/DC buck converters. The three-phase currents in any individual motor are equal in magnitude and phase, resulting in zero average torque production from the four motors during the charging mode of operation. This solution is significantly more expensive than previous option and can only be used when four in-wheel motors are envisioned.

An interesting solution based on an axial flux permanent magnet (PM) machine has been described in [45], and is shown in Fig. 5. It also integrates the existing propulsion

equipment into the charging process, where the charger is mounted on an electric scooter. The three-phase inverter is used as a single switch when charging. The lower IGBTs connected to the negative DC-bus are concurrently switched, while keeping the upper ones in the off state. Due to the utilization of the three IGBTs in parallel, current flow through these parallel branches will be the same. As a result, a reduction in conduction losses and an increase in efficiency are likely achieved. However, extra components are added such as a power rectifier and an LC line filter.

In [45], experimental verification is carried out using a 6kW axial flux PM machine, a 180V-12Ah lead-acid battery pack and a 50A-600V IGBT drive with a switching frequency of 25kHz. Moreover, an auxiliary 12V battery is used to supply the drive and control circuit. The latter is charged through a small size DC/DC converter fed from the drive battery during both traction and charging modes. Despite the above-mentioned advantages of this charger, it is unidirectional and is limited to slow charging. A similar solution has recently been introduced in [46], however, it employs an interior permanent magnet (IPM) propulsion drive as well as lithium-ion (Li-Ion) batteries with a bidirectional DC/DC conversion stage. A power factor correction (PFC) boost rectifier is achieved with additional hardware. This solution requires no passive elements, offers potential unity power factor operation, and limits harmonic content. The IPM drive
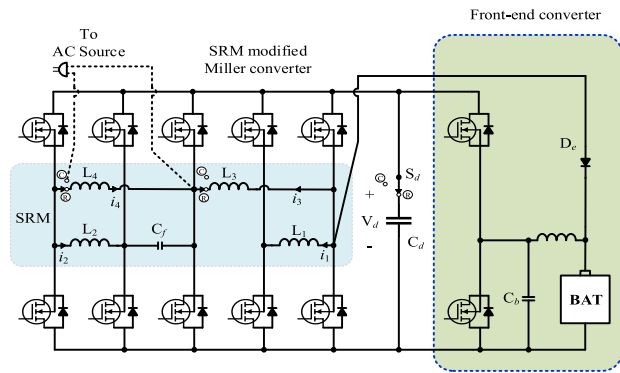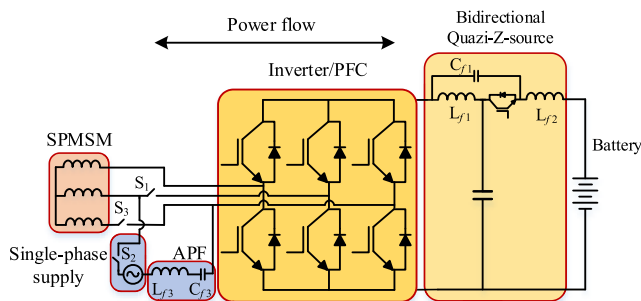
FIGURE 6. SRM-based integrated on-board charger.

FIGURE 7. Single-phase integrated charger with APF.

also provides improved performance during propulsion when compared to an IM or surface-mounted PM machine.

An integrated on-board battery charger using a switched reluctance motor (SRM) is described in [47]. It employs a four-phase SRM along with an improved converter [48] in addition to two intelligent power modules. These two intelligent modules form the SRM electrical drive using five inverter legs. Additionally, bidirectional power flow is possible using the additional leg acting as DC/DC converter. The main function of the buck-boost converter is to adjust the DC-bus voltage during motoring mode, while it is disabled during charging. The charger is suitable for both low-speed and high-speed applications but with simple modifications. Moreover, a power factor correction (PFC) control is performed. Fig. 6 presents the block diagram of the SRM-based integrated battery charger and motor driver. Accordingly, the ©symbol refers to charging position while, the ®symbol refers to propulsion position.

A single-phase integrated OBC charger achieving a power factor of 0.992 has been presented in [49]. The proposed topology comprises: a single-phase inverter, a bidirectional Quasi-Z-source converter, an active power filter (APF) and a single-phase surface-mounted permanent magnet synchronous (SMPMS) machine, as depicted in Fig. 7. During charging, the inverter in association with an inductor and capacitor are used to construct the APF. The APF integration considerably reduces the charger size, especially the capacitor size that is mainly responsible for smoothing the dc output

voltage. Furthermore, the APF removes the second-order harmonic content. During the propulsion process, S1 and S2 are switched ON, while S3 is OFF. Once S1 and S2 are switched OFF with S3 ON, the converter can be connected to a single-phase supply and the charging process starts. The main drawback of the topology is the use of passive elements (L, C) to construct the APF circuit.

Various topologies based on multiphase (greater than three) machines are discussed in [50]–[52], as shown in Fig. 8. These topologies can support either slow single-phase charging or fast three-phase charging. The proposed system in [50] considers a non-isolated solution for the slow charging of EVs that incorporates a nine-phase machine. While the one presented in [51] introduces an isolated system located outside the vehicle, that employs a six-phase machine (both symmetrical and asymmetrical configurations, which are explained later in the following subsection). A five-phase machine approach (non-isolated method) is utilized in [52]. Zero average torque production during the charging process is concurrently achieved with unity power factor operation at the grid side by all previous topologies.

In the case of an integrated OBC based on a nine-phase machine in [50], no hardware reconfiguration is necessary between the propulsion and charging modes of operation. On the other hand, the proposed systems in [51], [52], which are based on a six-phase machine and five-phase machine respectively, require hardware reconfiguration. The concept in [51] uses four additional switches in order to achieve hardware reconfiguration, while only two switches are used in [52].

An efficiency analysis of the various integrated charger topologies shows that a nine-phase charger corresponds to the highest efficiency (reaching 86% during the charging mode). During charging, the efficiency varies from 79% to 86% based on the applied topology. While, the efficiencies are slightly higher, between 81% and 89%, during the V2G mode.

B. FAST THREE-PHASE CHARGING
Fast battery charging can be achieved using either dc (off-board) or three-phase charging, as depicted in Table 1. Recent literature has introduced many topologies for IOBCs that offer fast battery charging by simply connecting the vehicle to three-phase mains. An interesting high-power integrated charger that supports fast three-phase charging has been described in [53] and is shown in Fig. 9. In this case, ac three-phase mains is connected to the mid-points of each winding of a three-phase machine (IM or PM) through an electromagnetic interference (EMI) filter and other protection devices. The main function of the EMI filter is to reduce high-frequency electromagnetic noise [54]. No additional components are required. The three-phase machine is connected to three H-bridges (also known as a six-leg inverter) followed by a front-end converter and a battery. The existence of the DC/DC conversion stage leads to a dramatic increase in silicon surface ratio (SSR) when compared to the case in which
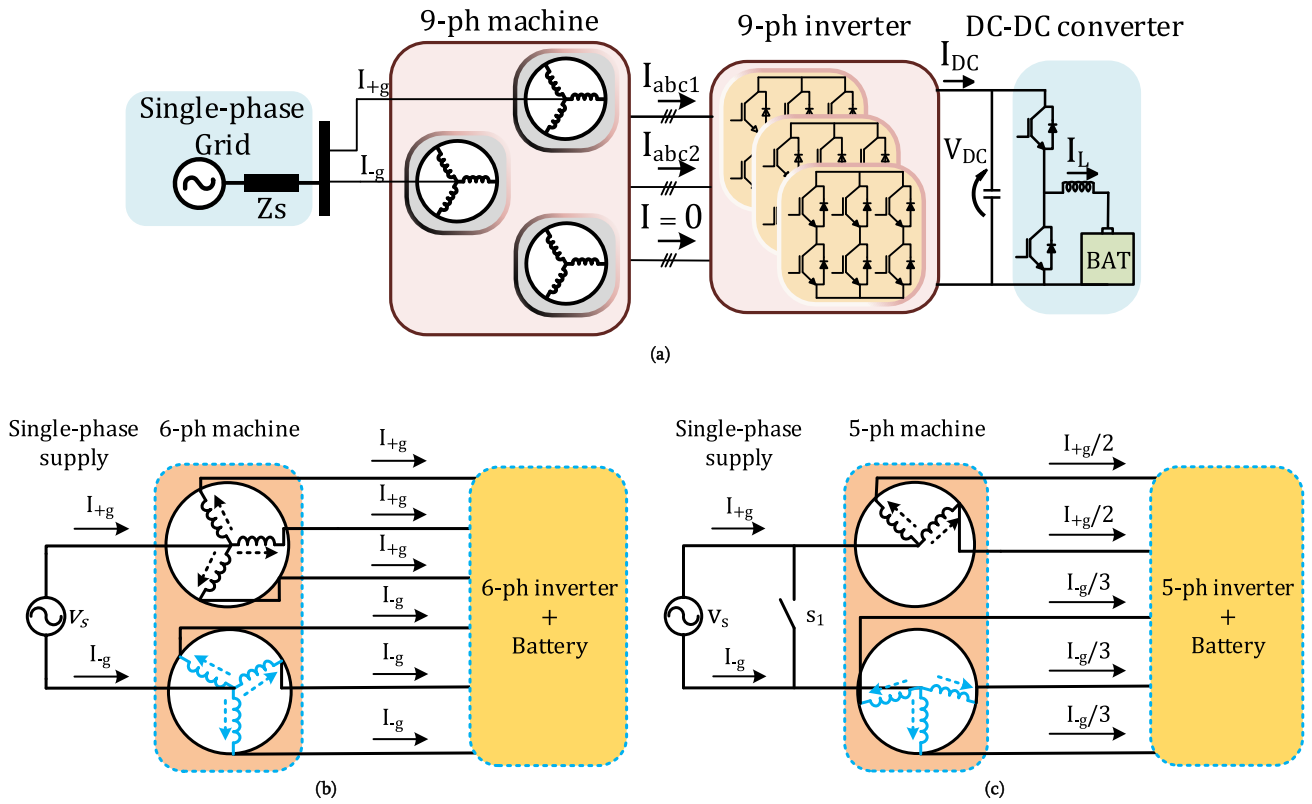
FIGURE 8. Topologies of integrated single-phase battery chargers employing: (a) a nine-phase machine, (b) a six-phase machine, and (c) a five-phase machine.
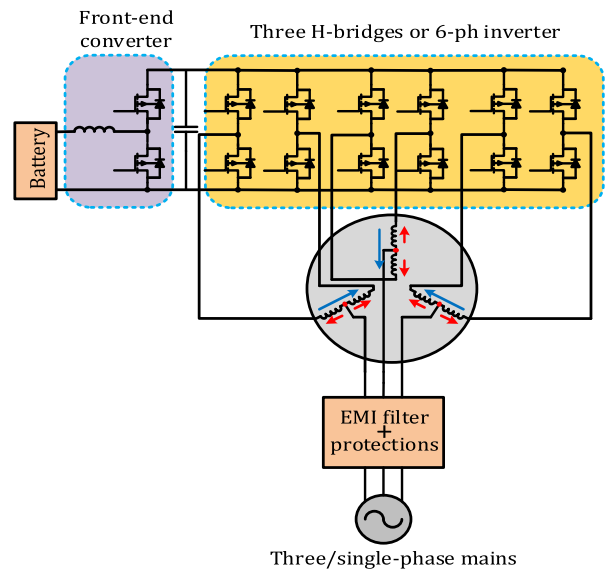

FIGURE 9. High power integrated charger on the basis of split-phase machine.

FIGURE 10. Air gap magnetizing flux distribution: (a) during propulsion mode. (b) during charging mode.

the inverter is directly fed by the battery. No hardware reconfiguration is required to change from one mode of operation to another.

During the charging process, the 6-phase inverter acts as a boost rectifier with PFC capability. The currents flow-
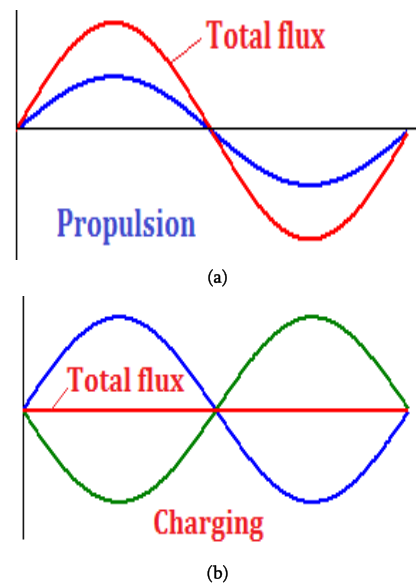
ing in each winding of the employed machine are equally split in two opposite directions. The currents in each coil cancel the effect of the other on the MMF. The MMF along the whole stator is, therefore, eliminated. As a result,
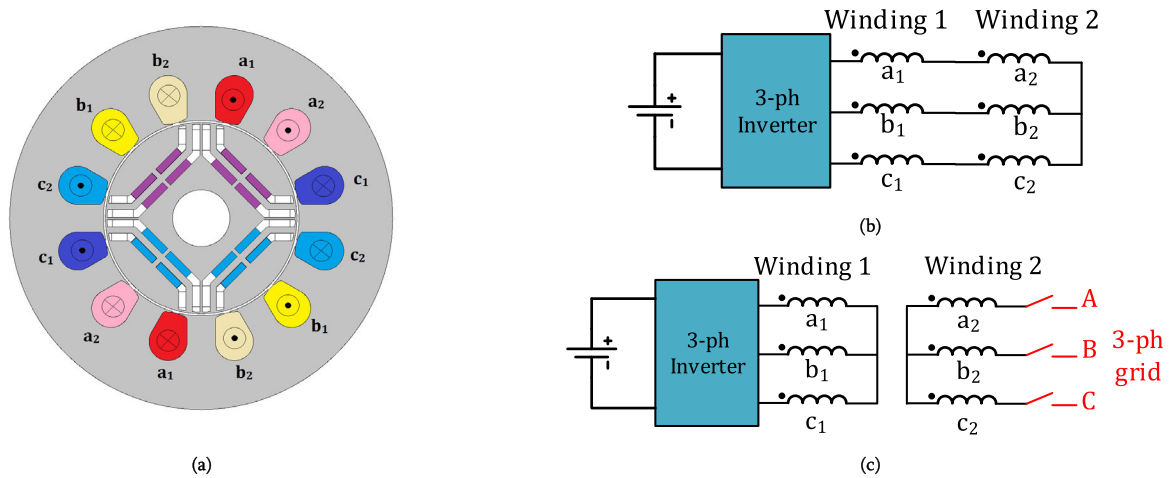
FIGURE 11. Isolated onboard charger based on PMSM: (a) winding configuration. (b) Arrangement of stator winging sets during motoring. (c) Arrangement of stator winging sets during charging.
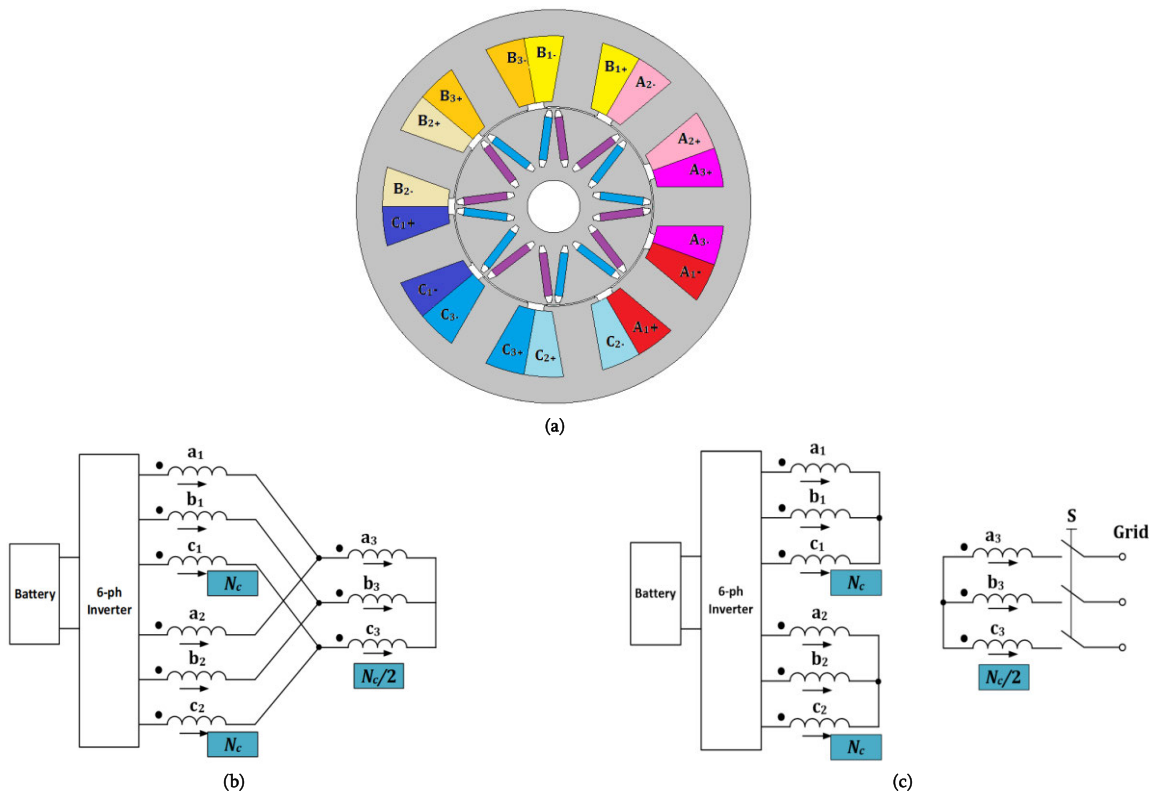

FIGURE 12. Isolated 9-phase 6-terminal on-board battery charger. (a) Winding layout. (b) Propulsion mode. (c) Charging mode.

the magnetic coupling between the rotor and the stator is lost. Fig. 10 presents the flux distribution: (a) during the propulsion mode and (b) during the charging mode. Although the rotor is at standstill, slight vibrations may occur due to space harmonics if permanent magnets are employed. Moreover, the total air gap magnetizing flux will ideally be zero and the machine equivalent inductance as seen from the grid side will be equal to the winding leakage inductance, which may not be sufficient for achieving high quality grid currents if a

distributed stator winding is employed. As a matter of fact, the winding leakage inductance (including zero-sequence) mainly depends on the winding layout; therefore, a particular winding configuration is necessary. Several solutions employing the same arrangement are presented in the literature [55]–[58]. Charging from both single-phase (slow) and three-phase (fast) grid is applicable with some modifications such as the use of only two H-bridge inverters, as well as two coils of the machine [56]. The main disadvantages of
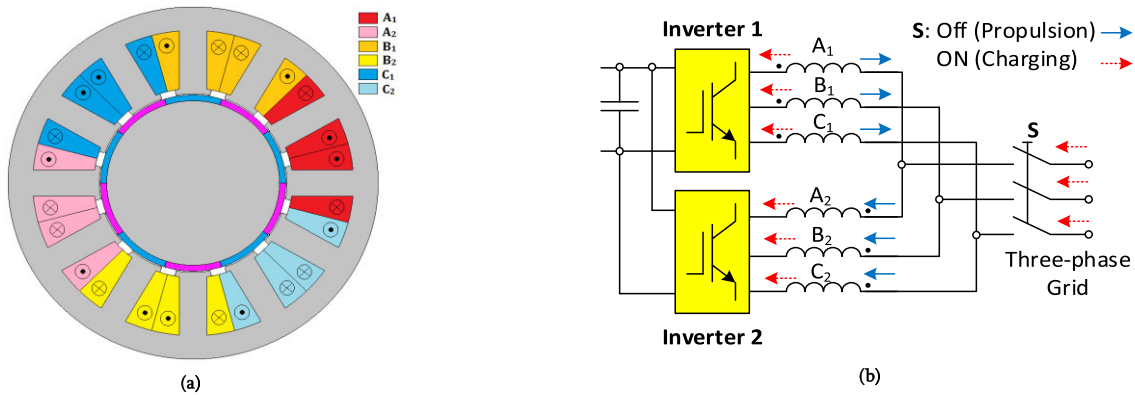
FIGURE 13. Integrated on-board battery charger utilizing PM machine with FSCW. (a) Winding arrangement. (b) Equivalent scheme during both charging and motoring mode of operation.

the proposed topology are the control complexity and the relatively low stator leakage inductance if machines with distributed windings are utilized.

An isolated charger that employs a PMSM with two three-phase stator winding sets is manifested in [59], as depicted in Fig. 11. The two separate winding sets are connected in series while the propulsion mode is activated, as shown in Fig. 11(a). On the other hand, the two three-phase winding sets act as a rotating transformer during charging mode. Initially, the inverter side three-phase winding set (Winding 1 in Fig. 11(b)) is used to synchronize the rotor with the grid and a mechanical clutch disconnects the motor from the mechanical transmission. The grid side winding (Winding 2) is connected to the grid upon synchronization, and consequently, the machine will act as a three-phase to three-phase rotating transformer. Battery charging is controlled using the three-phase inverter based on the induced three-phase voltages across Winding 1. Since the voltage is halved compared to the propulsion mode, the maximum charging power is also limited to half of the rated motoring power.

An isolated solution using an interior permanent magnet (IPM) machine has recently been investigated in [13] using a novel nine-phase six terminal stator winding layout as shown in Fig. 12. The high phase order improves the machine fault-tolerance under both motoring and charging modes, and allows for a limp home mode, where the machine can still run with a whole three-phase inverter disabled. It adopts a 9-slot/8-pole combination, or its multiples, with a FSCW. The system is more advantageous to a conventional three-phase one having the same slot/pole combination because the average torque is increased by 3% and torque ripple is dramatically decreased by 35%, if for no other reason than because of the suppression of MMF subharmonics. A similar connection was introduced for a high-power multiphase induction machine in [12], [60]. This study showed that the nine-phase six-terminal connection corresponds to a lower copper loss and a higher produced torque under various modes when compared to an asymmetrical six-phase one.

An integrated on-board battery charging system that employs a surface-mounted PM machine with a FSCW arrangement is discussed in [61]. A 12-slot/10-pole combination, which is shown promising for EV applications, is, therefore, adopted. The proposed charger consists of dual three-phase stator windings, two three-phase voltage source inverters (VSIs), a switch, and a battery, as depicted in Fig. 13. In motoring mode, switch S is off, and the two three-phase stator winding sets are connected in series. Two VSIs feed the two winding sets of the stator. This connection is similar to an open-end three-phase winding which results in better voltage waveforms as well as high reliability. During charging, switch S is on, the grid is connected to the two bidirectional converters after synchronization. The grid line current is shared by the two three-phase winding sets and the relative current directions between the two winding sets is reversed compared to the propulsion mode. Although the torque producing flux component should be nullified, similar to the topology given in Fig. 9, the other sub and super space harmonics contribute to the total equivalent stator inductance, leading to improved filtering of the grid charging current, when compared to a conventional distributed winding. The average torque production should be zero with a very low torque ripple component. Unity power factor operation at the grid side can also be ensured.

One of the major drawbacks of high phase order converters is the relatively higher number of semiconductor switches and the complexity of the corresponding driving circuit. The literature has, therefore, introduced several reduced-switch-count converters to overcome this drawback. An interesting solution that utilizes a nine-switch converter (NSC) along with the machine winding is presented in Fig. 14 [62]. This charger topology employs a symmetrical six-phase machine with zero torque production during charging mode, while unity power factor operation is obtained at the grid side. Moreover, the phase transposition principle was not needed for this case [63]. During the motoring mode, the six-phase machine with two isolated neutral points is fed from the NSC which simply acts as a six-phase inverter, by closing
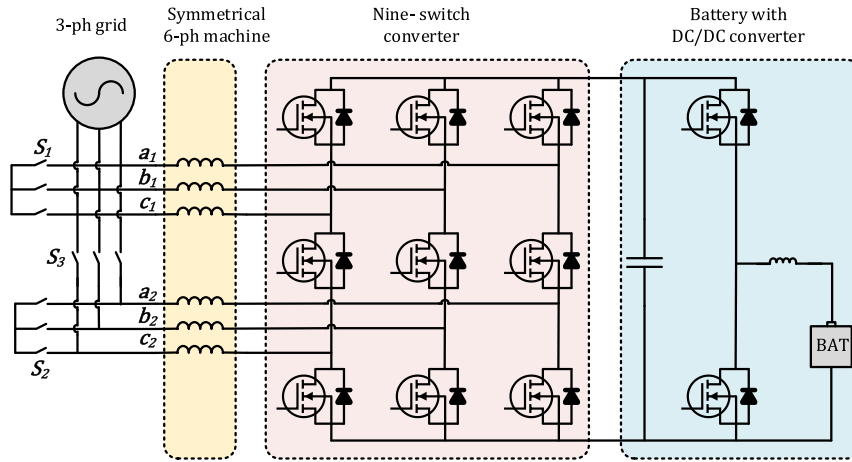
FIGURE 14. Integrated charger based on six-phase nine-switch converter.
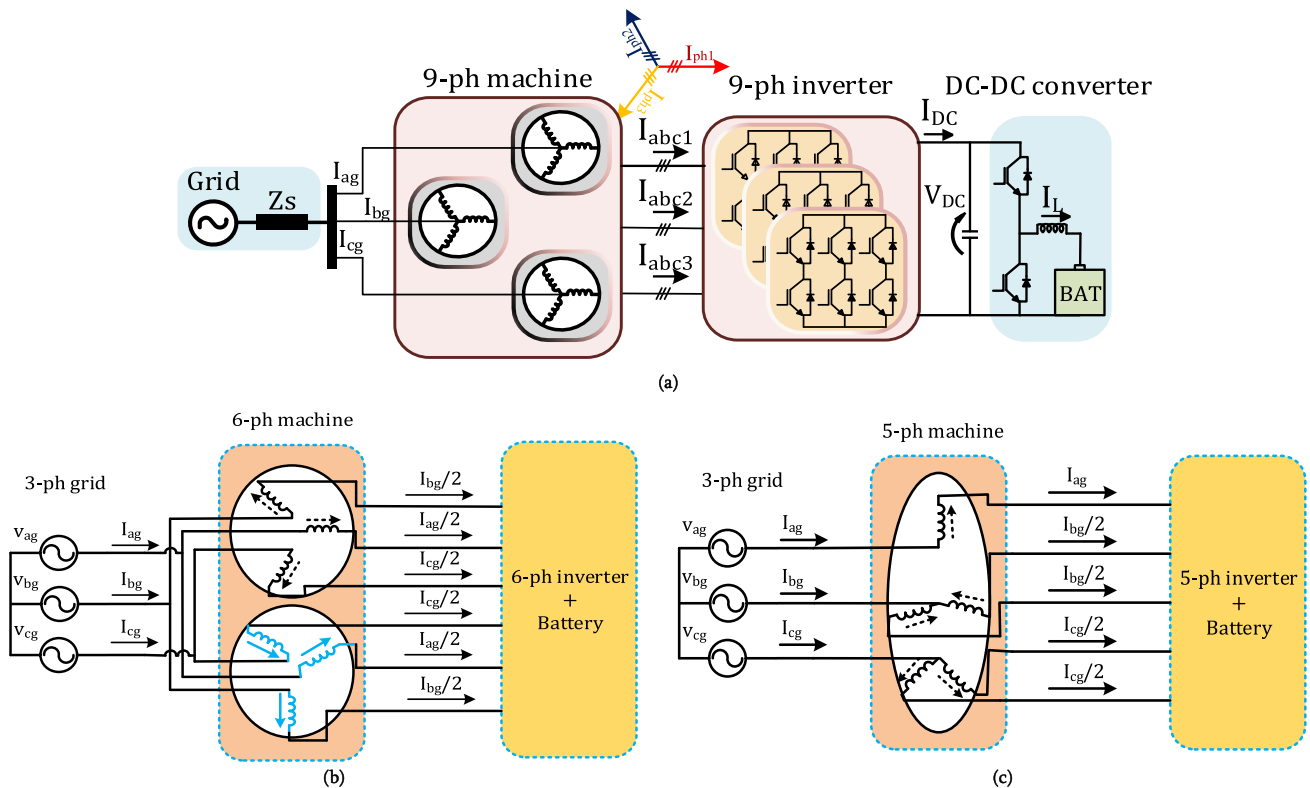

FIGURE 15. Topologies of integrated three-phase battery chargers employing: (a) a nine-phase machine, (b) a six-phase machine, and (c) a five-phase machine.

S1 and S2 with S3 open. When these switches change their conditions, the charging mode is initiated and the NSC acts as an active rectifier. The six-phase windings are, therefore, used as the grid-side filters. Despite the above-mentioned advantages of the topology, hardware reconfiguration between the propulsion and charging mode is needed and is executed using three additional switches.

Additionally, the relatively low dc-link utilization of NCSs generally stands as a challenging drawback of such a topology.

The topologies introduced in [50]–[52] are based on fast three-phase charging, and they are depicted in Fig. 15.

The investigated topologies typically comprise a multiphase machine, multiphase inverter, battery, and DC/DC converter. The operating principles, advantages, and limitations of these systems have been already stated in the previous section. The isolated chargers described in the previous subsection, incorporating either symmetrical or asymmetrical six-phase configurations are shown in Figs. 16 and 17, respectively.

Another solution that offers the cheapest integration technique with a charging power equal to motoring power is discussed in [64]. The topology uses a six-phase machine (non-isolated system), with zero average torque during the charging mode of operation. Unity power factor operation
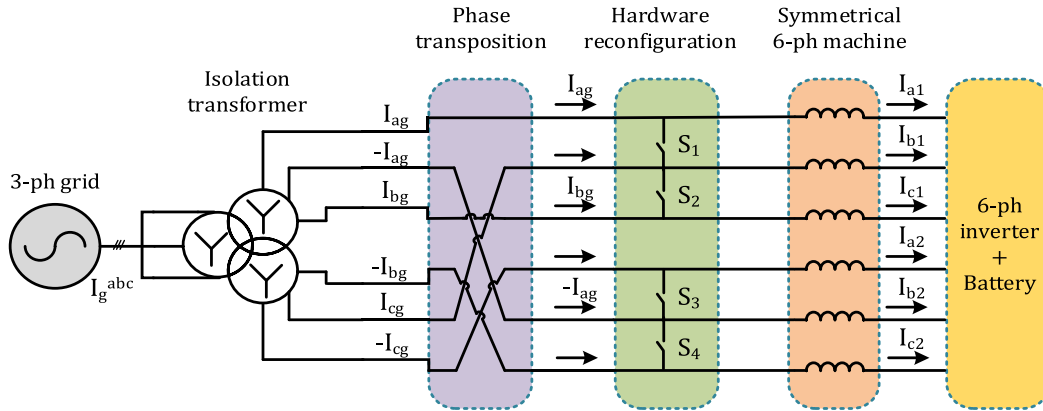
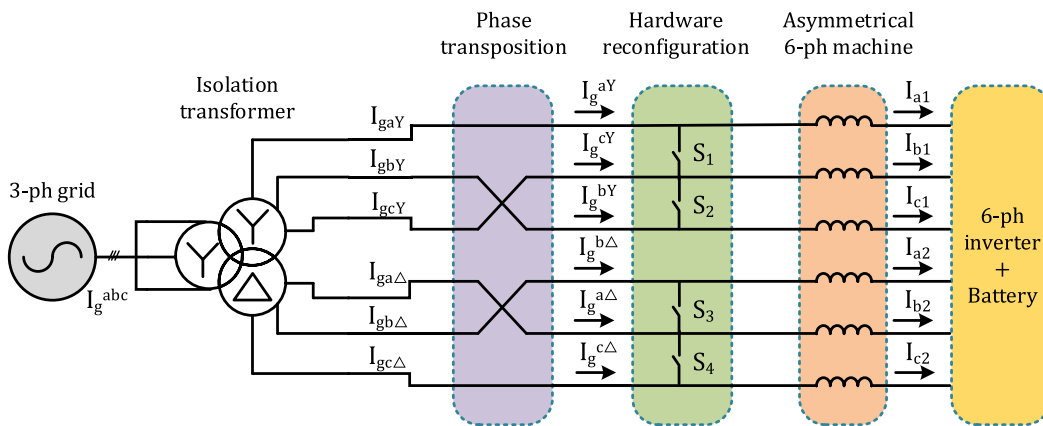**FIGURE 16.** Isolated charger using symmetrical six-phase topology.

FIGURE 17. Isolated charger using asymmetrical six-phase topology.

at the grid side is also guaranteed. However, hardware reconfiguration is considered as the main drawback of the topology. Whereas, the one in [65] employs an asymmetrical six-phase induction motor with the option of two-source charging through the integration of a photovoltaic (PV) based energy source. Newly added techniques to eliminate torque production during the charging operation on the basis of multiphase machine degrees of freedom have been investigated in [66], [9].

Although most of the previous topologies were mainly based on multiphase stator windings, recent literature has also proposed some alternative topologies compatible with the off-the-shelf three-phase based drivetrains. However, this entails extra hardware components to achieve the previously mentioned charging requirements. A simple solution that employs an additional three-phase interface converter to obtain a high-power three-phase integrated on-board charging has been investigated in [67] and is shown in Fig. 18. An additional three-phase interface converter is used to avoid hardware reconfiguration. The proposed charger is more advantageous than conventional ones (with the same ratings) because it allows charging at a high-power level with moderate size and weight. Moreover, it may be considered as a cost-effective

solution due to the omission of a second conversion stage [68]. At full load, the power factor at the grid side is almost unity and total harmonic distortion (THD) reaches 4.77% with an efficiency up to 92.6%. An innovative charger that underpins the same concept has also been presented earlier in [8]. It supports single-phase charging using an add-on diode instead of the three-phase interface converter with an efficiency reaching 93.1%.

Other solutions have been introduced in the available literature based on direct DC charging. In this context, a DC supply-based integrated OBC is depicted in Fig. 19 [69].

The proposed topology has significant advantages including charging at several voltage levels (higher or lower than the battery voltage), simultaneous motoring/charging operation, and bidirectional power flow with fault tolerant capability. Therefore, the cost of charging is significantly reduced. Besides, the proposed configuration can be applied to both three-phase and multiphase topologies employed for EV applications. The machine windings are utilized for filtration during the charging process. In addition, zero average torque production can be ensured.

Another three-phase integrated charger that adopts a novel technique for charging the battery without changing the motor
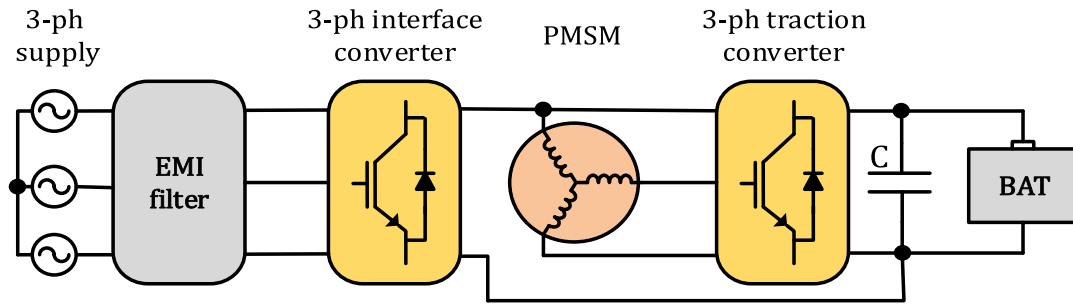
FIGURE 18. High-power three-phase integrated charger.
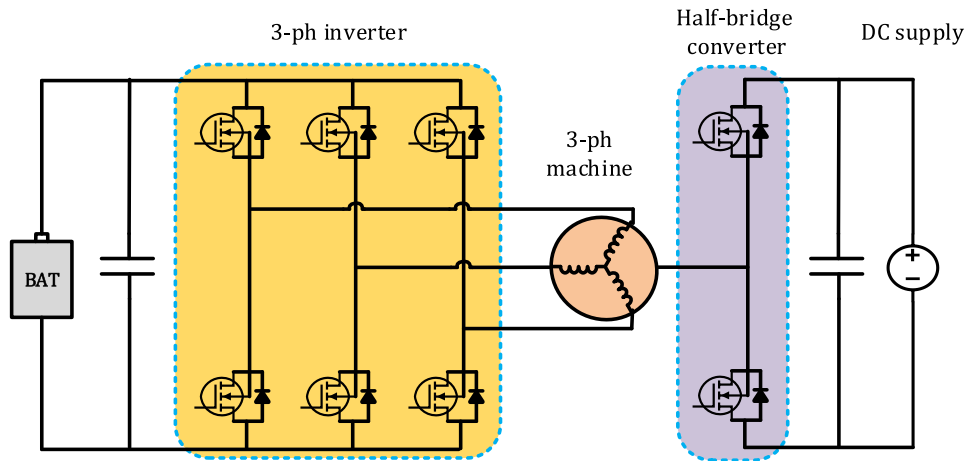
FIGURE 19. Fast integrated charger based on DC supply.
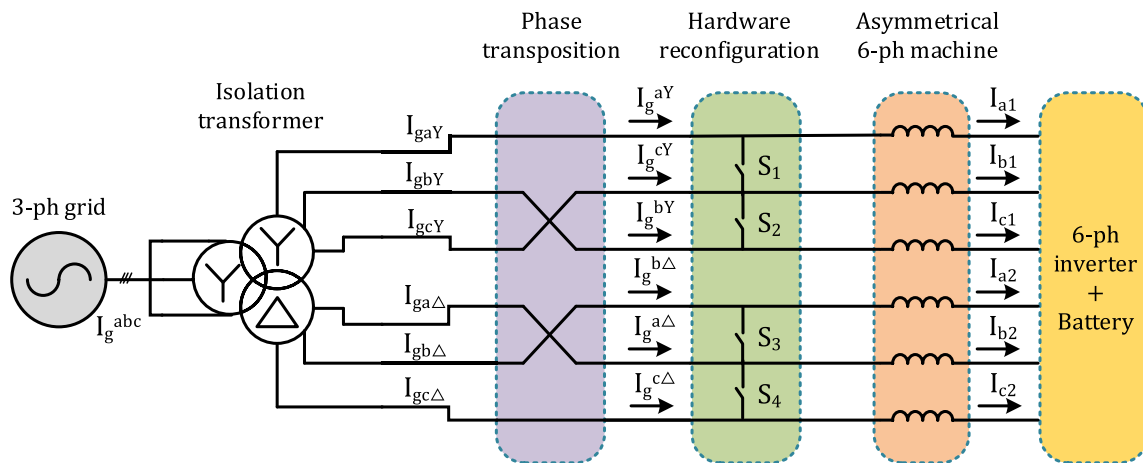
FIGURE 20. Fast integrated charger based on two-level DC converter.

winding connection is shown in Fig. 20 [70]. The suggested charger utilizes dual inverters which allows multilevel operation while employing a two-level three-phase VSI. It allows a buck-boost operation at unity power factor as well. Simply, the motor windings are integrated into a current source rectifier topology and behave as DC inductors. The control technique ensures the intermediate storage which is a critical aspect of the rectifier by utilization of motor windings. In this manner, the dual inverters and rectifier are synchronized

together through different modes of operation. However, this topology entails an extra current source converter for the charging process, which adds to the total system cost.

C. FAST MULTIPHASE CHARGING
The previous sections discussed the charging of EVs using either the single-phase or three-phase grid. Another solution is to connect the EV to a multiphase supply, which seems

FIGURE 21. Topologies of integrated multiphase charging: (a) a six-phase machine. (b) a five-phase machine.

to be a rather theoretical idea that can only be applied in practice upon the availability of such supplies. From the practical point of view, a multiphase voltage source can be obtained using either a three-phase to n-phase transformer [71], [72] or power electronic converters [73], [74]. Integrated chargers employing a multiphase voltage source are manifested in [75]–[77], and their proposed 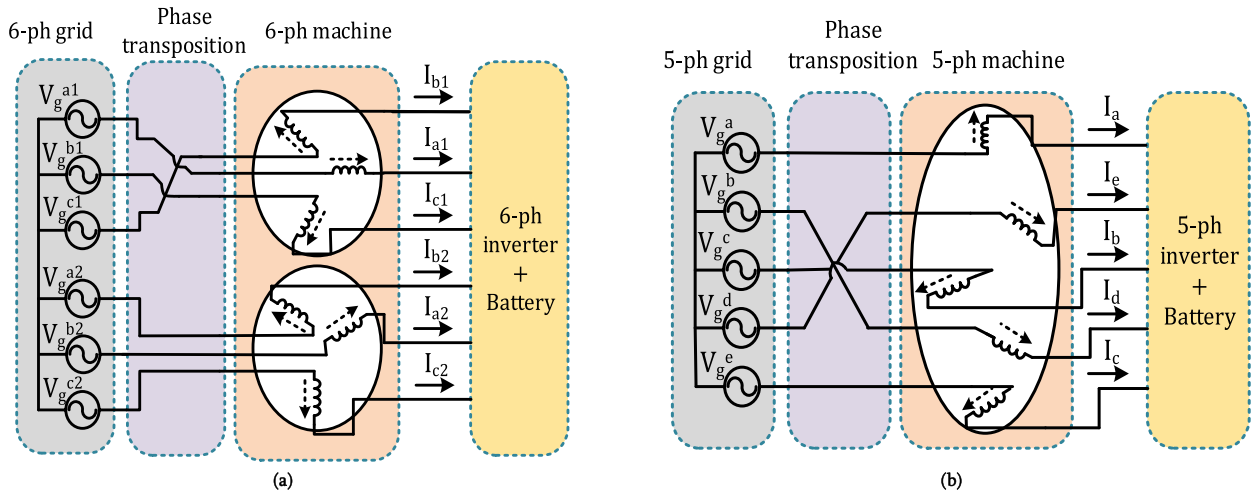configurations are depicted in Fig. 21. Integrated chargers on the basis of an asymmetrical six-phase [75], a five-phase [76], and a symmetrical six-phase [77] power supply are demonstrated in the literature. Whilst, isolated asymmetrical and symmetrical six-phase voltage sources are presented in [51]. Unity power factor operation at the grid side is ensured. The phase transposition block, shown in Fig. 21, is required to interconnect the machine terminals to the grid since the phase order will be different under both modes of operation (propulsion and charging modes) in order to excite the proper machine subspace under each mode [63]. The presented cases in Fig. 21 are given for charging mode only, where the machine secondary subspace is excited to ensure zero average torque production, while enabling power exchange between battery and grid.

To sum up the different aspects of the previously mentioned topologies, all addressed topologies are compared according to the number of machine phases, number of converter legs, average torque production during the charging process, hardware reconfiguration between the propulsion and the charging mode, galvanic isolation, pulsating torque, and the charging power as a ration of the propulsion power. The broad comparison of these topologies is revealed in Table 3.

III. CONTROL ALGORITHMS
This section sheds light on the common charging control techniques of integrated OBCs based on multiphase machines. All battery chargers are generally based on the so-called con-

stant current–constant voltage (CC-CV) approach. The system controller is similar to a grid-tie inverter controller, where the machine winding acts as an integrating filter inductance. The machine connections given in Fig. 15 ensure zero net magnetizing flux, and hence, zero-torque production. Either PQ control or voltage-oriented control is applied to charge the battery pack under constant current or constant voltage, respectively. In the former technique, the dq grid current components are set based on the required reference charging current magnitude and the intended grid power factor. While in the voltage-oriented control approach, the reference *dq* current components are obtained based on the dc-link voltage error and the desired grid power factor. The inner current controller structure will, however, differ based on the available supply, namely fast three-phase charging or slow single-phase charging, as shown in Fig. 22.

A. THREE-PHASE CHARGING
In three-phase charging, the machine stator winding is reconfigured based on the available number of phases to integrate the power converter with the grid, while ensuring a nullified net flux inside the machine core during charging. For the multiphase based integrated OBC system, which is the main target of this study, this can be carried out using two current control techniques. The first current control technique assumes that grid line currents are equally shared among the converter legs (Figs. 15(a) and (b) for the nine-phase and six-phase based OBCs, respectively). Hence, the system can be regarded as an equivalent three-phase grid connected inverter. This assumption, however, discards possible mismatches between phases, which may be a challenge to achieve in practice. The controller block diagram for this case is shown in Fig. 22(a). First, the grid currents (i_g^{abc}) are transformed into their synchronous reference frame components (i_{dg}, i_{qg}) using Park's transformation. Considering that all variables must be synchronized with the grid phase voltage,

TABLE 3. Broad comparison of various topologies of integrated chargers.

Ref.	Fig.	No. of machine phases	Type of supply	No. of converter legs	Charging with zero torque production	Pulsating torque	Charging power to propulsion power	Hardware recon-figuration needed	V2G	Galvanic isolation
[40]	1	3	1-ph	4	Yes	Yes	33%	Yes	Yes	No
[41]	2	3	1-ph	6	Yes	No	100%	No	Yes	No
[43]	3	3	1-ph/ 3-ph	3	Yes	No	100%	Yes	Yes	No
[44]	4	3	1-ph	12	Yes	No	100%	No	Yes	No
[45]	5	3	1-ph	3	Yes	No	100%	Yes	No	No
[49]	7	3	1-ph	3	Yes	Yes	50%	Yes	Yes	No
[50]	8(a), 15 (a)	9	1-ph/ 3-ph	9	Yes	No	100%	No	Yes	No
[64]	8 (b), 15 (b)	6	1-ph/ 3-ph	6	Yes	Yes	100%	Yes	Yes	No
[51]	16, 17	6	1-ph/ 3-ph	6	Yes	No	100%	Yes	Yes	Yes
[52]	8 (c), 15 (c)	5	1-ph/ 3-ph	5	Yes	Yes	60%	Yes	Yes	No
[53]	9	3	1-ph/ 3-ph	6	Yes	No	100%	No	Yes	No
[59]	11	6	3-ph	3	No	No	50%	Yes	Yes	Yes
[61]	13	6	3-ph	6	Yes	No	100%	No	Yes	No
[13]	12	9	3-ph	6	No	No	33%	Yes	Yes	Yes
[62]	14	6	3-ph	3	Yes	No	100%	Yes	Yes	No
[67]	18	3	1-ph/ 3-ph	2 × 3	Yes	No	100%	Yes + Extra converter	Yes	No
[69]	19	3	DC	4	Yes	No	100%	No + Extra leg	Yes	No
[70]	20	3	3-ph	3 VSI + 3 CSI (Charging)	Yes	No	100%	No	No	No

a Phase-Locked Loop (PLL) is utilized to obtain the grid angular position (θ_s^*). Ultimately, the reference value of the direct component (i_d^*) is adjusted according to the desired charging level, while the reference value of the quadrature component (i_q^*) is set to zero to guarantee unity power factor operation at the grid side. Then, the *dq* current errors are used to derive the reference voltage components $\left(v_d^*, v_q^*\right)$ using two PI controllers. The reference voltage components are transformed back to their three-phase components using the inverse Park's transformation to formulate the reference voltage of the PWM. Considerable constant current is supplied to the battery till it reaches 80% of its full capacity. To fully charge the battery, the reference power is set to about 10% of its initial value to complete the rest of the charging process, as thoroughly explained in [78]. Under the voltage-oriented control method [79], the battery is charged with a constant maximum current until reaching the cut-off voltage, which is

a predefined threshold value known as a safety limit at which constant voltage (CV) control begins. The charging curve is depicted in Fig. 23. In CV mode, the voltage across the DC-link is maintained constant until the current drops to preset minimum values from its maximum indicating a full charge is fulfilled [80]. Typically, these values depend on the battery type.

On the other hand, the second current control approach exploits the additional machine subspaces to charge the battery through the non-torque-producing subspaces, while controlling the torque producing current components $(i_{\alpha\beta1})$ to zero. Although this current control technique offers superior performance, it corresponds to a more complex current controller. As an example, the current controller for a nine-phase system based on vector space decomposition (VSD) is shown in Fig. 22(b). The nine-phase currents are decomposed into four decoupled subspaces and a single unidirectional
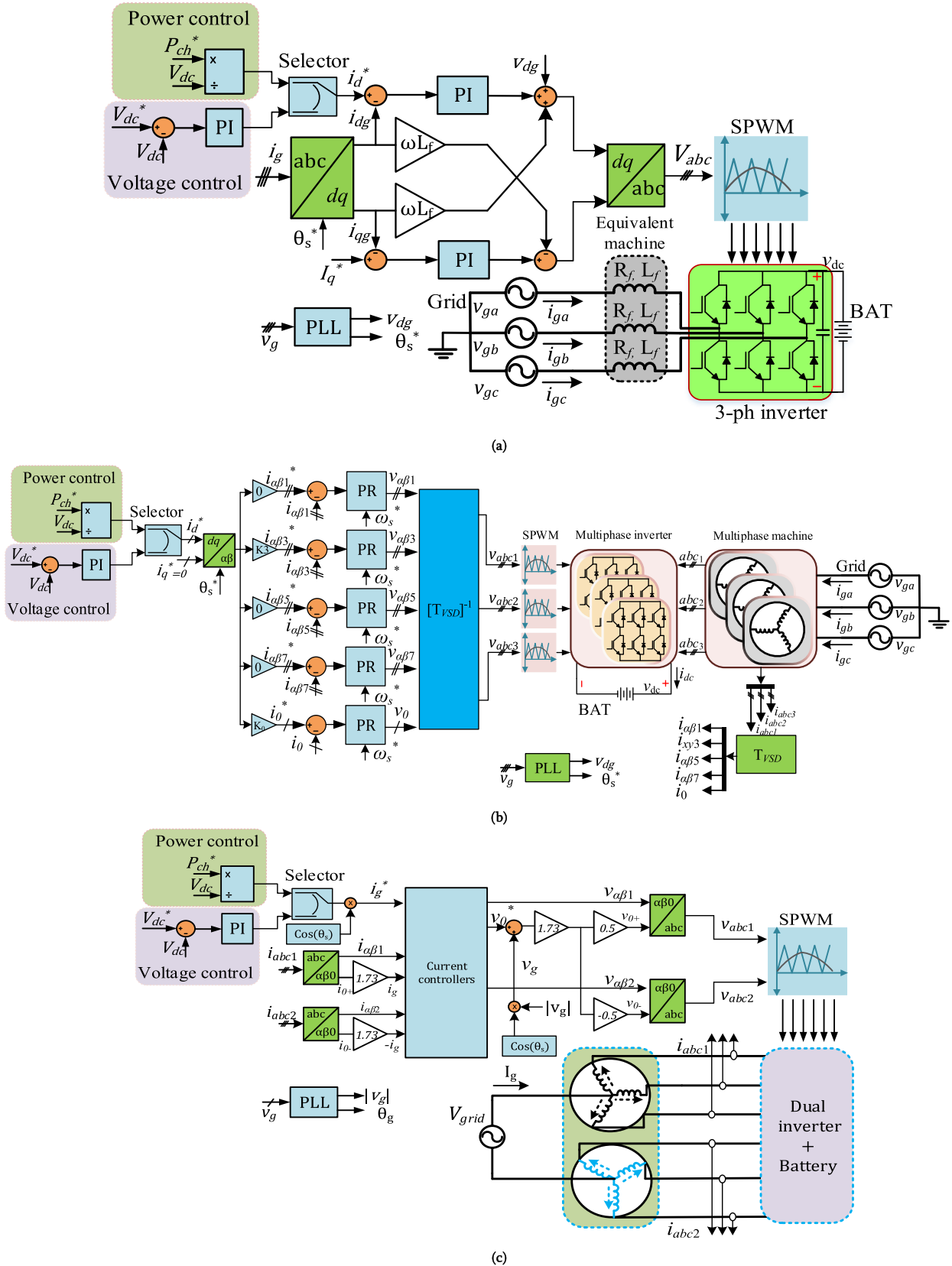
FIGURE 22. Charging control: (a) Three phase charging based on equivalent three-phase grid connected inverter. (b) Three phase charging using VSD based current control (c) Single-phase charging.
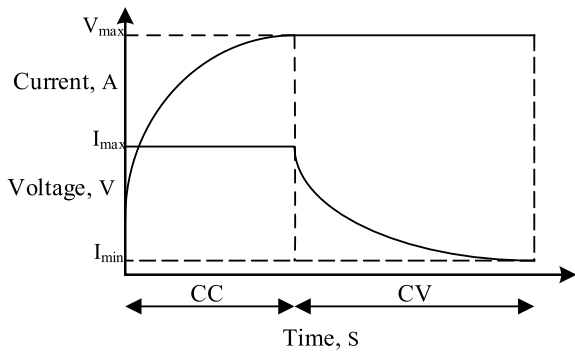
FIGURE 23. Battery charging characteristic curve.

zero sequence component. The torque/flux production is regulated by controlling the $\alpha\beta_1$ subspace. Balanced three-phase grid currents can be ensured by controlling the current components of the subspace $\alpha\beta_3$ and the zero sequence current component based on the desired charging current level [50]. All other sequence current components should be controlled to zero during charging, which entails a total of nine current controllers (the first technique corresponds to two current controllers only).

B. SINGLE-PHASE CHARGING

In single-phase charging, the OBC system is regarded as a single-phase grid connected inverter. For multiphase-based integrated OBCs, the charging current is regulated by controlling the zero-sequence current component of the stator currents of the different three-phase sets. The controller block diagram is shown in Fig. 22(c), which is applicable to all topologies given in Fig. 8 [37]. Unlike three-phase charging, the battery current under single-phase charging will experience a pulsating current component at double the line frequency, which has been addressed using innovative converter topologies in [49]. The voltage-oriented control technique can also be utilized for single-phase charging taking into account that there is no decoupling transformation applied to either the grid voltage or the machine currents.

IV. DESIGN CONSIDERATION OF INTEGRATED OBCS EMPLOYING MACHINES WITH FSCW

PM machines with a FSCW arrangement have shown outstanding merits in recent studies when compared to conventional machines having DW layouts. Fractional slot windings are broadly categorized into non-overlapped concentrated (FSCW) and overlapped (doubled through) windings. Several FSCW layouts have shown promise in EV applications due to their myriad advantages. These advantages include high slot fill factor, low cogging torque [81], short end turns, high efficiency, and flux weakening capability [82], [83]. On the other hand, the air gap flux distribution of FSCWs is extremely distorted due to different sub and super space harmonics with relatively high magnitudes [26], [27]. As an illustrative example, the layouts of two machines with DW and FSCW

and having the same rotor poles are shown in Figs. 24(a) and 24(b), respectively, along with their MMF distributions. Clearly, the resultant MMF distribution of FSCW is highly distorted with respect to the high-quality MMF distribution of the DW layout. Different space harmonics induce excessive eddy currents in the rotor core. The resultant power losses by these induced eddy currents severely affect the rotor magnets, since it is very hard to release the heat from the rotor, which may cause thermal demagnetization [27]. Also, the interaction between these low order harmonics causes audible noise and vibrations in the mechanical structure [29]. In the available literature, the utilization of multiphase windings was adopted to mitigate the aforementioned demerits while increasing fault-tolerance capability [84]. However, more complicated power electronics converters will necessarily be required.

A FSCW refers to a winding having a fractional number of slots per pole per phase, q, given by (1). While, a DW corresponds to an integral q. The realization of balanced windings in case of symmetrical multiphase machines depends on the condition given in (2).

$$q = \frac{S}{2p.m} \qquad (1)$$

$$\frac{S}{[GCD\,(S,\,2p)]} = mC \qquad (2)$$

where S is the number of slots, p number of pole pairs, C is a positive integer, m is the number of phases, and GCD is the Greatest Common Divisor. The procedure of selecting an optimal layout of a three-phase concentrated windings was presented in [85]. Furthermore, it was expanded to include multiphase concentrated winding configurations (for e.g. 4, 5, and 6 phases) in [25]. As far as the rotor eddy current losses are concerned for this winding layout, many models were introduced to compute the rotor losses [86], [87], while some other indices were introduced to assess the severity of this loss component for a given winding design [88].

Since the machine is an essential element in integrated OBCs, the effect of the adopted winding layout should be carefully considered. This point has not been comprehensively addressed in the available literature so date. Most of the available systems produced in early studies were adopting machines with double layer windings. A common assumption that has been widely used is the zero/neglected flux production under charging mode.

However, this assumption cannot, in principle, be generalized for FCSW layouts. Although the torque producing flux component can be nullified under charging mode, the MMF spectrum will still be showing space harmonic components with relatively high magnitudes [61], which may have serious effects during the charging process. In this section, different slot/pole combinations that have been shown in literature as viable selections for EV applications are investigated under both motoring and charging modes of operation. The induced eddy current rotor losses have been used as a potential qualitative measure to compare different topologies. From the
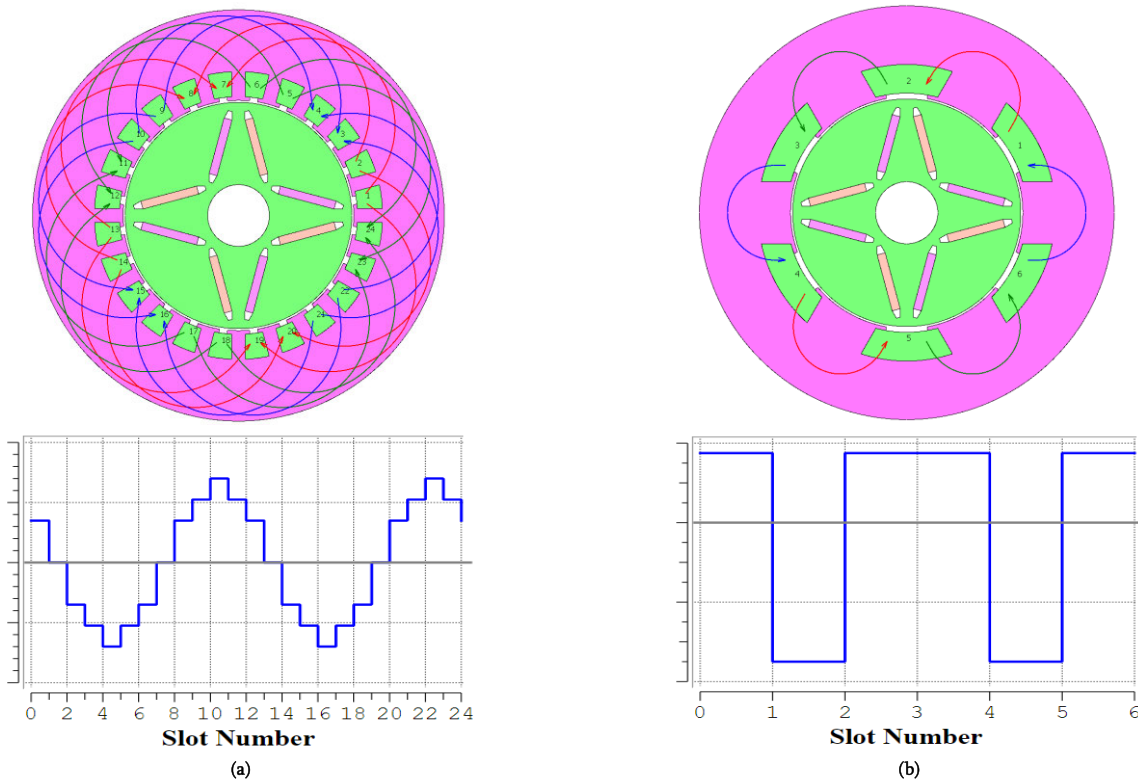
FIGURE 24. Winding layouts with corresponding MMF distribution. (a) DW layout 24-slot/4-pole combination. (b) FSCW layout 6-slot/4-pole combination.

authors' viewpoint, the most promising layouts for integrated OBCs, among the previously introduced topologies in the previous section, are those based on six-phase and nine-phase layouts, which facilitate the employment of the well-established three-phase based converters with no/limited extra hardware components. Hence, the study herein is limited to these phase orders and their possible winding layouts, namely, symmetrical six-phase, asymmetrical six-phase, dual three-phase, symmetrical nine-phase, and asymmetrical nine-phase layouts. A selection criterion of the optimal slot/pole combinations, which seemly optimize the machine performance in terms of core losses under both charging and propulsion modes of operation, is also introduced. Moreover, in this section, the effect of using the stator shifting on slot harmonics suppression will be investigated for some slot/pole combinations as a comparison between the non-overlapped FSCW and overlapped fractional slot windings. The latter layout has shown promise to significantly suppress the induced rotor losses [89], [90].

A. ROTOR LOSS INDEX FOR DIFFERENT SLOT/POLE COMBINATION AND DIFFERENT NUMBER OF PHASES

Various slot/pole combinations have been introduced in the literature employing three-phase [91], four-phase [25], five-phase [89], and six-phase [25] configurations. Due to the above-mentioned benefits of multiphase machines over their three-phase counterparts, this study addresses optimal combinations of slot and pole numbers for multiphase machines

that can practically/easily be utilized as a viable drivetrain for available EV designs, namely six-phase and nine-phase designs.

As a rule of thumb, the number of stator slots should be an integer multiple of the number of phases, while the number of poles is preferably selected as $2p = S \pm 1$ or $2p = S \pm 2$ with regard to odd and even number of slots, respectively. The selection of a suitable FSCW slot/pole combination is subject to many factors such as machine winding factor, torque ripple magnitude, rotor losses, noise and vibration. These factors are presented comprehensively in the literature [92]–[95]. The winding factor (k_w) of the torque producing MMF component, which is likely not the fundamental component when a FSCW is applied, should be as close to unity as possible. The higher the winding factor is, the higher the effective number of turns will be. Accordingly, the torque density is enhanced. Low cogging torque is a distinguishing feature of a good PM machine design. The machines with a higher lowest common multiple (*LCM*) between their slot and pole numbers offer lower cogging torque [25]. So, the number of poles is selected to be closer to the number of slots to maximize the *LCM* (*S*, $2p$). The greatest common divisor (*GCD*) of the number of slots and poles represents the machine symmetry and is preferred to be an even number to avoid unbalanced magnetic pull. The *GCD* (*S*, $2p$) should also be maximized to decrease the net radial force. Hence, noise and vibrations produced by the net radial force will likely be reduced.

TABLE 4. Six-phase FSCW configurations.

Ref.	Slot/pole combination	k_w	LCM	GCD	Possible topologies	R_i-Propulsion	R_i-Charging	Prospective topology
[98]	6/4	0.866	12	2	Dual	13.6897	14.2458	
[98]	6/8	0.866	24	2		47.4525	9.1709	
[30]	12/10	0.966	60	2	Dual or Asymm	7.3303/ 6.4018	9.0147/ 5.8493	
[92]	12/14	0.966	84	2		13.586/ 12.4978	6.9182/ 4.2823	
[32, 99]	24/10	0.925	120	2	Dual or Asymm	1.916/ 1.1225	14.1514/ 5.8876	
[97, 100]	24/14	0.759	168	2	Dual or Asymm	1.6125/ 1.0122	5.5385/ 4.6788	
[101]	18/16	0.945	144	2	Dual	4.3158	5.2488	Figures 7(b)/10/12 13/16(b)
[101]	18/20	0.945	180	2		7.0568	4.3257	
[102, 103]	24/22	0.983	264	2	Dual or Asymm or Symm	2.6704/ 2.3255/ 3.7427	3.5117/ 3.5971/ 4.4650	
[102, 103]	24/26	0.991	312	2		4.0106/ 3.6872/ 5.5506	2.8361/ 3.1663/ 3.6531	
[25]	30/28	0.951	420	2	Dual	1.6167	2.2826	
[25]	30/32	0.951	480	2		2.3067	1.8804	
[104]	36/34	0.9525	612	2	Dual or Asymm or Symm	0.9819/ 1.0381/ 1.4050	1.4669/ 2.0716/ 1.8363	
[104]	36/38	0.9525	684	2		1.3558/ 1.2173/ 1.8826	1.239/ 1.6237/ 1.5626	

TABLE 5. Nine-phase FSCW configurations.

Ref.	Slot/pole combination	k_w	LCM	GCD	Possible topologies	R_i-Propulsion	R_i-charging	Prospective topology
[13]	9/8	0.945	72	1	Asymm	10.8049	8.5467	
[105]	9/10	0.945	90	1		16.5733	7.2649	
[84, 106]	18/8	0.9452	72	2	Asymm	1.8567	9.5243	
[33]	18/10	0.9452	90	2		2.0908	4.5445	
[31]	18/16	0.945	144	2	Asymm	3.6716	2.3315	Figures 7(a)/11/16(a)
[31]	18/20	0.945	180	2		6.4028	2.2926	
[107]	27/26	0.954	702	1	Asymm	1.9752	2.9699	
[107]	27/28	0.954	756	1		2.4626	2.6748	
[104, 108]	36/34	0.953	612	2	Asymm	0.8137	0.9162	
[104, 108]	36/38	0.953	684	2		1.1948	0.8283	

Rotor losses induced by the MMF harmonic content constitute the major disadvantage of FSCW-based PM machines. The rotor loss index (R_i) has been introduced in literature to assess the rotor loss impact of different slot/pole combinations and is governed by (3) [87];

$$R_i = \sum_v \frac{\xi^4}{\sqrt[4]{\left(\xi^4 + \pi^4\right)}} \left(\frac{k_{wv}}{k_w}\right)^2 \frac{v}{p} k_{gap} \qquad (3)$$

where v is the harmonic order, ξ is the specific wavelength for each harmonic order, k_{gap} is the ratio of the air gap to rotor diameter, k_w the winding factor of the fundamental harmonic, and k_{wv} the winding factor of v harmonic order. The rotor index (R_i) is calculated based on the study in [87] and is extended herein to the six-phase and nine-phase machines with a further classification by possible six-phase and nine-phase configurations. The
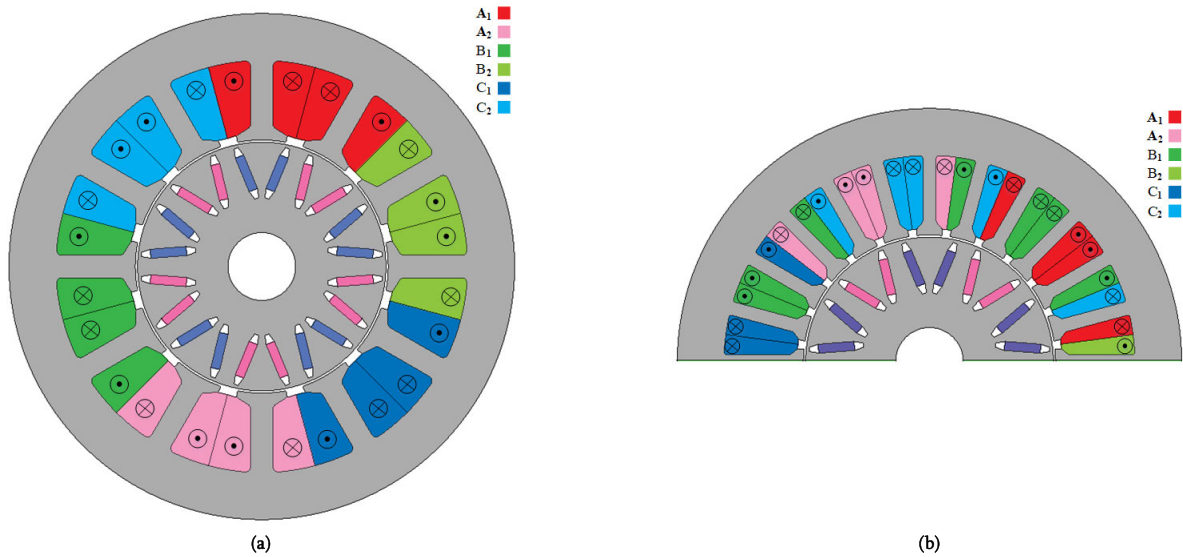
(a)

(b)

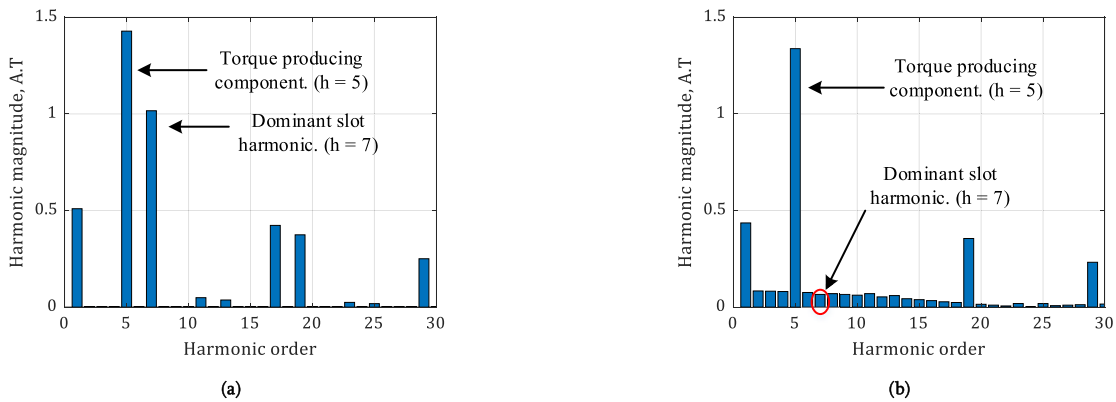**FIGURE 25. Dual three-phase winding layouts. (a) 12-slot/10-pole. (b) 24-slot/10-pole.**

(a)

(b)

FIGURE 26. MMF harmonic spectra for a dual three-phase winding configuration under propulsion mode. (a) 12-slot/10-pole. (b) 24-slot/10-pole.
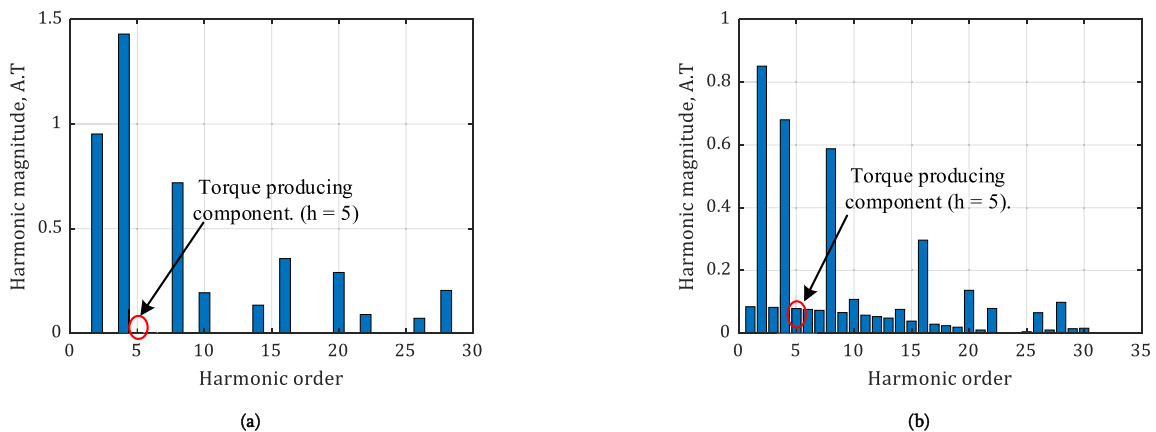

(a)

(b)

FIGURE 27. MMF harmonic spectra for a dual three-phase winding configuration under charging mode. (a) 12-slot/10-pole. (b) 24-slot/10-pole.

complete steps on how the rotor index is calculated can be found in [87].

Tables 4 and 5, respectively, present a comprehensive comparison between valid slot/pole combinations that can accom-

modate different six-phase and nine-phase configurations, addressing the synchronous winding factor (k_w), lowest common multiple [$LCM(S, 2p)$], and greatest common divisor [$GCD(S, 2p)$]. Moreover, the rotor index (R_i), which is a
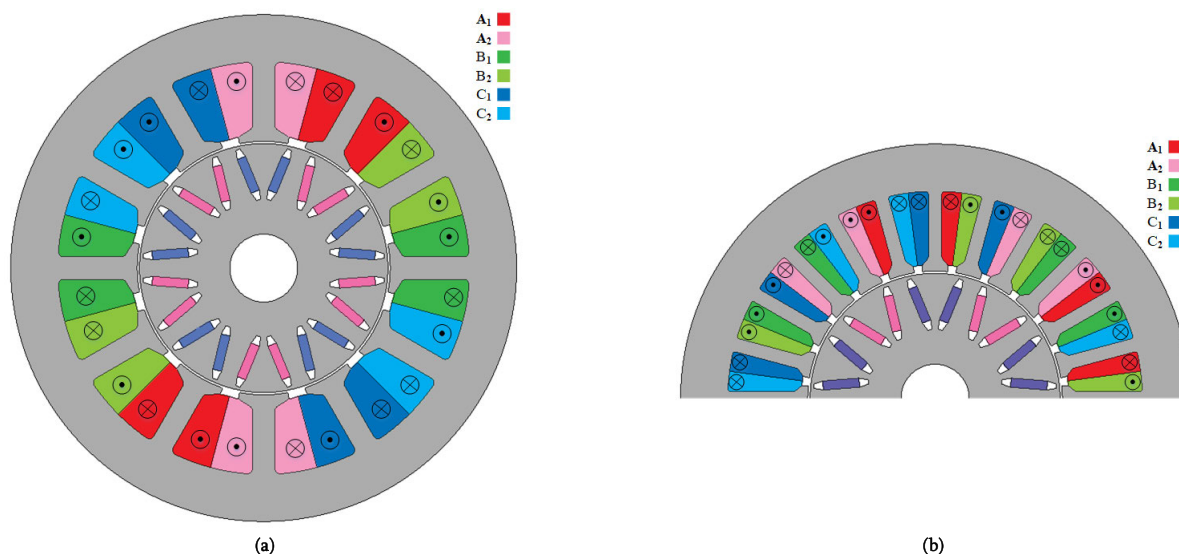
FIGURE 28. Asymmetric six-phase winding layouts. (a) 12-slot/10-pole. (b) 24-slot/10-pole.

FIGURE 29. MMF harmonic spectra for asymmetric six-phase winding configuration under propulsion mode. (a) 12-slot/10-pole. (b) 24-slot/10-pole.

FIGURE 30. MMF harmonic spectra for asymmetric six-phase winding configuration under charging mode. (a) 12-slot/10-pole. (b) 24-slot/10-pole.

notable contribution of this study, is calculated for each combination and different winding configuration. This is carried out for the three possible six-phase winding configurations, namely, symmetrical six-phase ($\delta = 60°$), asymmetrical six-phase ($\delta = 30°$), and dual three-phase ($\delta = 0°$) configurations, where δ is the spatial phase angle between the two

three-phase winding sets. For the nine-phase case, there are two possible topologies, namely a symmetrical ($\delta = 40°$) and an asymmetrical ($\delta = 20°$). The definition of a specific slot/pole combination viability is based on the corresponding star of slots [96], which is first determined based on motoring mode. For the same layout, the MMF spectra under both propulsion and charging modes are then obtained. To compare different possible slot/pole combinations equipped with a specific winding layout under both propulsion and charging modes, the rotor loss index defined in (3) is found to be suitable in this respect. The best compromise is the one which minimizes the losses under both modes. The given tables also include the possible converter topologies that can be used under different cases.

As is clear from Table 4, the following conclusions may be drawn:

- Some slot/pole combinations can accommodate only a single winding configuration (dual, symmetrical, or asymmetrical), while others can fit all possible configurations.
- The rotor index is significantly affected by the selected slot/pole combination. As the slot/pole combination increases, the rotor index will generally decrease. As an example, the rotor index under the propulsion mode is 6.4018 and 1.0381 for the 12-slot/10-pole and 36-slot/34-pole machines (with asymmetric six-phase configuration), respectively.
- Although the rotor index increases when the number of poles is higher than the number of slots during the propulsion process (e.g. the rotor index is 3.6716 and 6.4028 for 18-slot/16-pole and 18-slot/20-pole, respectively), the rotor index decreases during the charging process (e.g. the rotor index is 2.3315 and 2.2926 for 18-slot/16-pole and 18-slot/20-pole, respectively).
- It can also be concluded that the asymmetrical six-phase winding generally minimizes the rotor loss index under propulsion mode, thanks to its superior MMF spectra under this mode. The same conclusion cannot be generalized for the charging mode. This point will be verified in the following subsection.
- The concept of stator shifting [90], [97] has also shown promise to significantly suppress the induced rotor losses by simply doubling the number of stator slots for a given pole number, while the coil span is increased to two slots. As an example, by comparing the 12/10 and 24/10 combinations in Table 4, the rotor loss indices for both motoring and changing modes are significantly decreased for the 24/10 combination due to the significant reduction in the dominant slot harmonic. This case will also be presented in more details in the next subsection.

Table 5 shows the possible slot/pole combinations that can accommodate a nine-phase winding. Since a symmetrical winding can simply be deduced from the asymmetrical nine-phase by reversing the middle three-phase set, the given cases

are limited to asymmetrical nine-phase configurations. These have been favored in most available literature due to a better quality of flux distribution [50].

B. COMPARISON BETWEEN OVERLAPPED AND NON-OVERLAPPED FRACTIONAL SLOT WINDINGS

To further investigate the results given in Tables 4 and 5, the winding layouts and the corresponding MMF harmonic spectra of some selected cases are investigated, namely 12/10 and 18/16 for the six-phase and nine-phase configurations, respectively.

The 18/16 example is employed instead of the 9/10 combination, which may be considered as an impractical example due to the significant rotor losses and the unbalanced radial forces. The effect of stator shifting on the suppression of undesirable space harmonics will also be investigated using two examples, namely, 24/10 and 18/10 for the six-phase and nine-phase configurations, respectively.

Considerable reported work has been aimed at reducing the effect of eddy current loss, the associated noise, and undesirable vibration due to sub, super, and slot harmonics [90], [97], [109]. Compared to the different slot harmonics suppression techniques, the concept of stator shifting has recently been considered as the most effective solution to suppress the effect of slot harmonics [90], [97]. As a result of employing this technique, several interesting slot/pole combinations have shown promise in EV applications, namely 24-slot/10-pole [32], [99] and 18-slot/10-pole [33]. These slot/pole combinations are based on overlapped windings with a coil pitch of two. It can be noted from Table 4 that the rotor index under the propulsion mode (asymmetric configuration) is 6.4018 and 1.1225 for 12-slot/10-pole and 24-slot/10-pole, respectively. This yields a significant reduction in machine losses. Whereas, a slight difference in the rotor index can be noticed under the charging mode. To further investigate the reason behind this improvement, the MMF spectra of both windings are plotted.

Fig. 25 shows the FSCW winding configuration when applied to the 12-slot/10-pole and 24-slot/10-pole machines (dual three-phase configuration). The MMF spectra produced in the propulsion mode are shown in Fig. 26, where a substantial reduction in the dominant slot harmonic ($h = 7$) can be noticed for the 24-slot/10-pole machine when compared to the 12-slot/10-pole one. On the other hand, the torque producing component, $h = 5$, is completely cancelled under charging mode, as shown in Fig. 27. Therefore, zero average torque production during the charging process is guaranteed. Additionally, FSCW winding layouts for the 12-slot/10-pole and 24-slot/10-pole machines equipped with asymmetric six-phase configuration are presented in Fig. 28, while their MMF spectra under propulsion and charging modes are shown in Figs. 29 and 30, respectively. Clearly, the asymmetrical six-phase topology will suppress all sub harmonics under propulsion mode, which contributes to the reduction in rotor eddy losses. The same conclusion can be noted under charging mode.
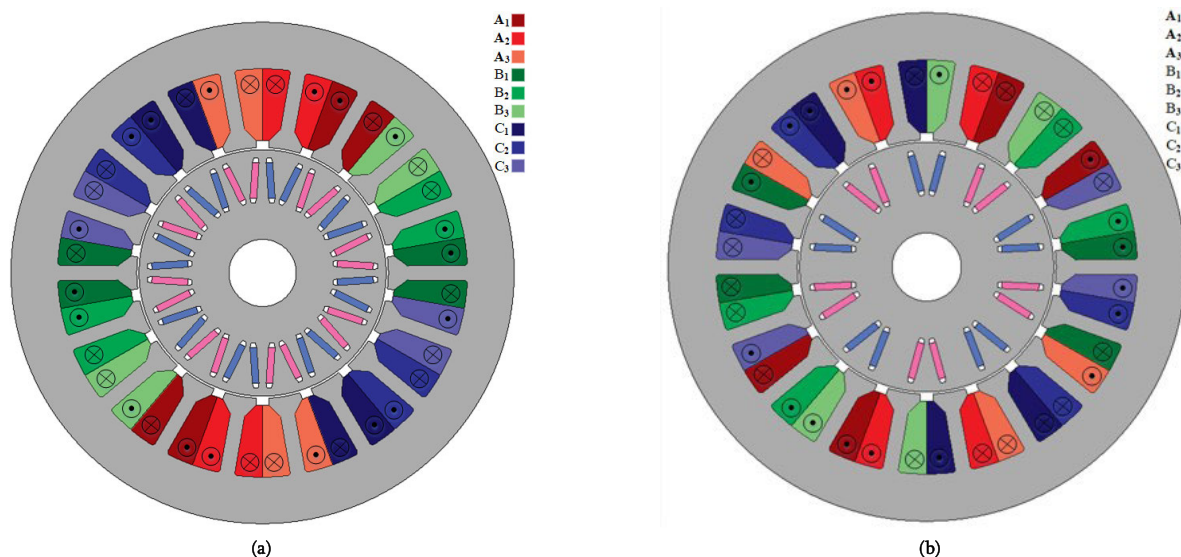
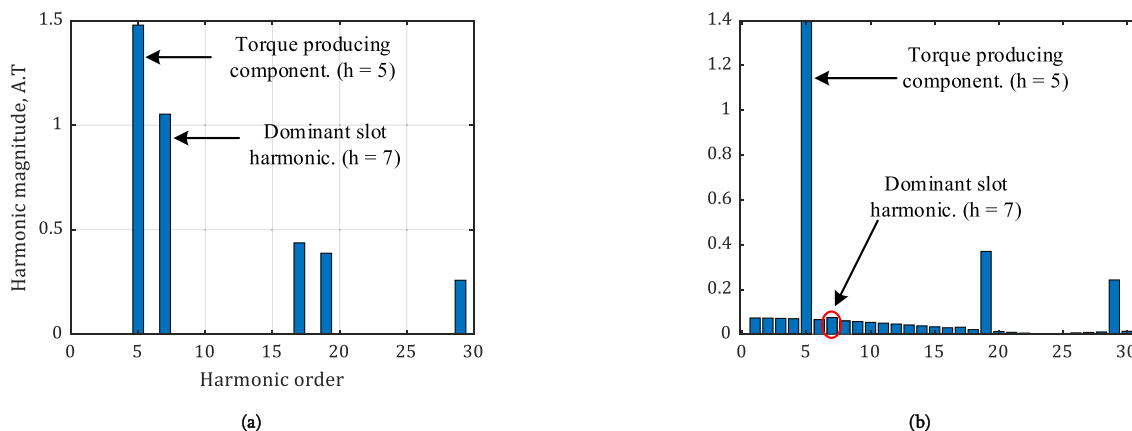**FIGURE 31. Asymmetric nine-phase winding layouts. (a) 18-slot/16-pole. (b) 18-slot/10-pole.**
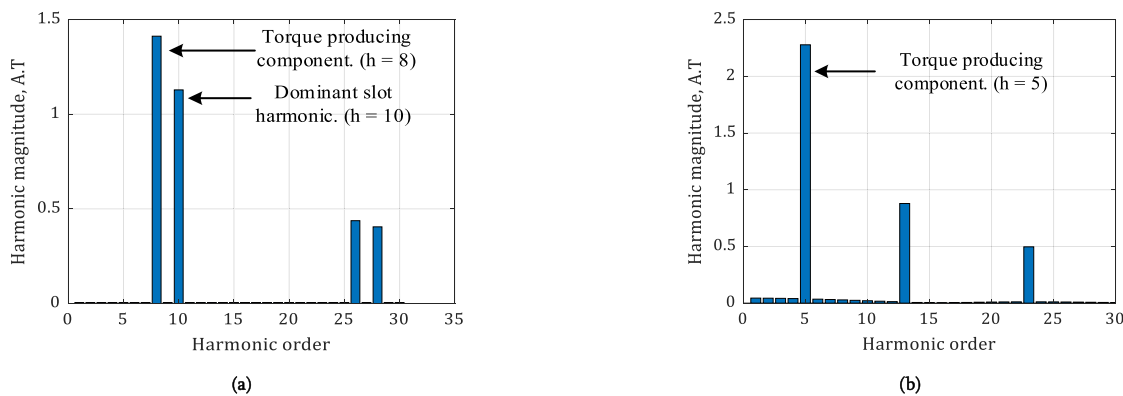
FIGURE 32. MMF harmonic spectra for asymmetric nine-phase winding configuration under propulsion mode. (a) 18-slot/16-pole. (b) 18-slot/10-pole.
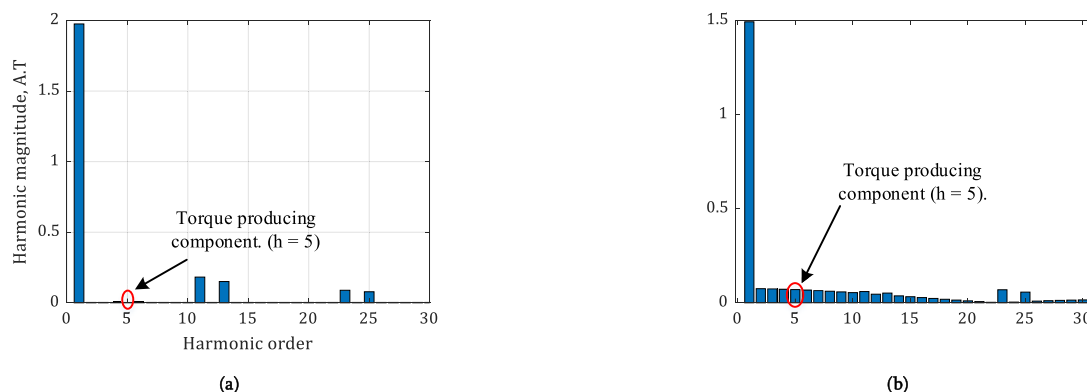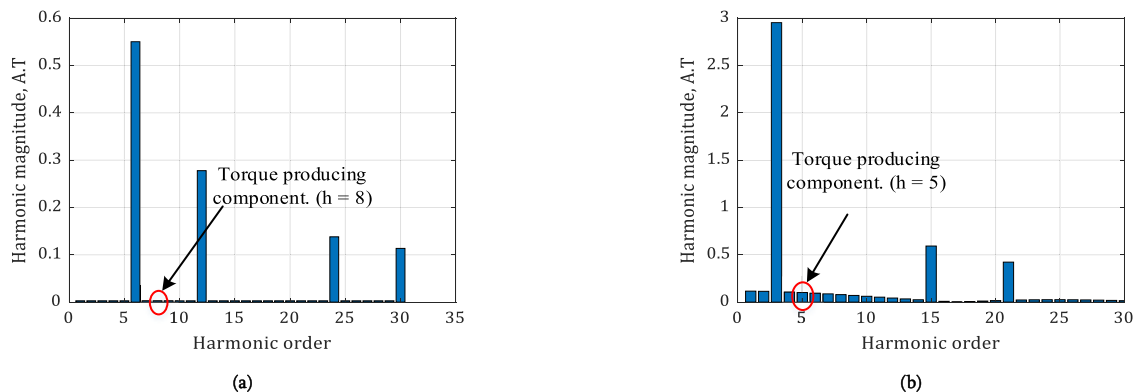

FIGURE 33. MMF harmonic spectra for asymmetric nine-phase winding configuration under charging mode. (a) 18-slot/16-pole. (b) 18-slot/10-pole.

For the 18-slot/16-pole and 18-slot/10-pole examples, the corresponding FSCW winding arrangements are shown in Fig. 31, while the MMF spectra for both motoring and charging modes are shown in Figs. 32 and 33, respectively. The 18/16 example represents a nonoverlapped winding layout, where the dominant slot harmonic ($h = 10$) is as high

as the torque producing component ($h = 8$). The asymmetrical winding configuration also suppresses all subharmonics, which adds to the total improvement in the induced eddy current losses when compared with conventional three-phase machines. Under charging mode, the torque producing component ($h = 8$) is completely cancelled, which ensures zero torque production under this mode of operation.

When comparing the 18/10 example having an overlapped winding layout, with the 9/10 case equipped with a single tooth (nonoverlapped) winding, the first slot harmonic ($h = 4$) is completely cancelled for the 18-slot/10-pole machine, which significantly reduces the machine eddy current loss and improves the overall efficiency. In charging mode, both sub and super harmonics are significantly reduced, which highly improves the machine core loss under this mode of operation. Other slot-pole combinations could also be investigated to maximize the machine performance, in terms of a higher torque density, lower magnet and core losses, a higher efficiency, an improved flux weakening capability, and an improved fault tolerant capability.

V. FUTURE RESEARCH TRENDS
This section forecasts the possible future research trends covering the main challenges and/or opportunities in the field of integrated OBC technology. The following aspects are identified as the major challenges in this context:

A. INTEGRATED OBCs ENHANCEMENTS
- Improving the charger reliability, durability, and safety through optimal design of different components.
- Performing additional functionalities in order to be compatible with smart grid functionalities [110].
- Optimization of V2G and G2V operational modes by employing information and communication enabling technologies [111].
- Maximizing the charging efficiency [39].
- Charging infrastructure/grid challenges for the various approaches.

B. CONVERTER TOPOLOGY ENHANCEMENTS
- Converter design considerations that benefit from, if necessary, new wide bandgap power devices [36], [110].
- Development of advanced converter topologies based on resonant converters in order to curtail the losses [112].
- Feasibility of contactless integrated OBCs.

C. MACHINE DESIGN ENHANCEMENTS
- Machine design considerations in integrated onboard charger applications to improve efficiency and reduce parasitic effects, especially when concentrated winding designs are employed.
- Reduction in the effect of eddy current loss, the associated noise, and undesirable vibrations due to sub, super, and slot harmonics.

- Experimental investigation of different slot/pole combinations commonly suggested for EV applications.
- Development of SRM-based integrated chargers that can be applied to low-speed applications.

D. CONTROLLERS ENHANCEMENTS
- Employing recent model-based current controllers instead of conventional PI-based control.
- Parameter resilience in advanced controllers.
- Charger compliance with grid standards.

VI. CONCLUSION
This paper surveyed the state-of-the-art in integrated on-board chargers for electric vehicle applications. Various types of chargers were discussed, while investigating their advantages and limitations. Additionally, different types of converters, drivetrains that are employed in EVs, charging control techniques, and technical challenges have been presented. Moreover, the employment of either three-phase or multiphase machines in slow (single phase) and fast (three-phase) charging was illustrated. Additionally, an analysis of FSCW PM machines, which are preferably proposed for EV application, was presented. In this study, various FSCW slot/pole combinations introduced in the literature for three-phase machines have been extended to six-phase and nine-phase topologies. These slot/pole combinations have also been compared based on screening factors and their harmonic spectra under charging and propulsion modes of operation. The rotor index, a quantitative measure of the rotor loss, was calculated for these different topologies. It has been concluded that the slot/pole combinations that accommodate asymmetrical six-phase winding topologies seem to be the best compromise minimizing the induced rotor losses under propulsion mode for all feasible slot/pole combinations, while possessing an acceptable value for the rotor loss index under charging mode. The concept of stator shifting is also effective to further reduce the induced losses under both charging and propulsion modes of operation.

REFERENCES
[1] IEA, "Global EV outlook 2019: Scaling-up the transition to electric mobility," OECD, Paris, France, 2019.

[2] S. Bala, T. Tengner, P. Rosenfeld, and F. Delince, "The effect of low frequency current ripple on the performance of a lithium iron phosphate (LFP) battery energy storage system," in *Proc. IEEE Energy Convers. Congr. Exposit. (ECCE)*, Sep. 2012, pp. 3485–3492.

[3] F. L. Mapelli, D. Tarsitano, and M. Mauri, "Plug-in hybrid electric vehicle: Modeling, prototype realization, and inverter losses reduction analysis," *IEEE Trans. Ind. Electron.*, vol. 57, no. 2, pp. 598–607, Feb. 2010.

[4] S. Haghbin, S. Lundmark, M. Alakula, and O. Carlson, "Grid-connected integrated battery chargers in vehicle applications: Review and new solution," *IEEE Trans. Ind. Electron.*, vol. 60, no. 2, pp. 459–473, Feb. 2013.

[5] M. Yilmaz and P. T. Krein, "Review of battery charger topologies, charging power levels, and infrastructure for plug-in electric and hybrid vehicles," *IEEE Trans. Power Electron.*, vol. 28, no. 5, pp. 2151–2169, May 2013.

[6] M. Y. Metwly, F. A. Maximos, A. T. Ahmed, A. S. Hawam, A. A.-M. Zaki, A. A.-M. Helal, A.-R.-M. Mokhtar, S. M. Abdelghaffar, R. A. Taha, R. A. Hamdy, and A. S. Abdel-Khalik, "Design case study of a nine-phase integrated on-board battery charger," in Proc. 20th Int. Middle East Power Syst. Conf. (MEPCON), Dec. 2018, pp. 815–821.

[7] K. Fahem, D. E. Chariag, and L. Sbita, "On-board bidirectional battery chargers topologies for plug-in hybrid electric vehicles," in Proc. Int. Conf. Green Energy Convers. Syst. (GECS), Mar. 2017, pp. 1–6.

[8] C. Shi, Y. Tang, and A. Khaligh, "A single-phase integrated onboard battery charger using propulsion system for plug-in electric vehicles," IEEE Trans. Veh. Technol., vol. 66, no. 12, pp. 10899–10910, Dec. 2017.

[9] Y. Xiao, C. Liu, and F. Yu, "An effective charging-torque elimination method for six-phase integrated on-board EV chargers," IEEE Trans. Power Electron., vol. 35, no. 3, pp. 2776–2786, Mar. 2020.

[10] J. de Santiago, H. Bernhoff, B. Ekergård, S. Eriksson, S. Ferhatovic, R. Waters, and M. Leijon, "Electrical motor drivelines in commercial all-electric vehicles: A review," IEEE Trans. Veh. Technol., vol. 61, no. 2, pp. 475–484, Feb. 2012.

[11] E. A. Grunditz and T. Thiringer, "Performance analysis of current BEVs based on a comprehensive review of specifications," IEEE Trans. Transport. Electrific., vol. 2, no. 3, pp. 270–289, Sep. 2016.

[12] A. S. Abdel-Khalik, S. Ahmed, and A. M. Massoud, "A nine-phase six-terminal concentrated single-layer winding layout for high-power medium-voltage induction machines," IEEE Trans. Ind. Electron., vol. 64, no. 3, pp. 1796–1806, Mar. 2017.

[13] A. S. Abdel-Khalik, A. Massoud, and S. Ahmed, "Interior permanent magnet motor-based isolated on-board integrated battery charger for electric vehicles," IET Electr. Power Appl., vol. 12, no. 1, pp. 124–134, Jan. 2018.

[14] S. R. Khayam Huseini, E. Farjah, N. Tashakor, and T. Ghanbari, "Development of an integrated switched-reluctance motor drive with battery charging capability for electric vehicle propulsion system," in Proc. 6th Power Electron., Drive Syst. Technol. Conf. (PEDSTC), Feb. 2015, pp. 579–584.

[15] J. Liang, W. Li, and Z. Song, "Control strategy of integrated charger base on split-winding switched reluctance motor drive," in Proc. 20th Int. Conf. Electr. Mach. Syst. (ICEMS), Aug. 2017, pp. 1–6.

[16] Y. Hu, C. Gan, Q. Sun, P. Li, J. Wu, and H. Wen, "Modular tri-port high-power converter for SRM based plug-in hybrid electrical trucks," IEEE Trans. Power Electron., vol. 33, no. 4, pp. 3247–3257, Apr. 2018.

[17] P. Dupuy, "Electric traction chain for an automobile," Google Patents 13 056 318, Aug. 4, 2011.

[18] I. Subotic, M. Jones, and E. Levi, "A fast on-board integrated battery charger for four-motor EVs," in Proc. Int. Conf. Electr. Mach. (ICEM), Sep. 2014, pp. 2066–2072.

[19] E. Levi, "Multiphase electric machines for variable-speed applications," IEEE Trans. Ind. Electron., vol. 55, no. 5, pp. 1893–1909, May 2008.

[20] A. S. Abdel-Khalik and S. M. Gadoue, "Improved flux pattern by third harmonic injection for multiphase induction machines using neural network," Alexandria Eng. J., vol. 50, no. 2, pp. 163–169, Jun. 2011.

[21] E. Levi, R. Bojoi, F. Profumo, H. A. Toliyat, and S. Williamson, "Multiphase induction motor drives—A technology status review," IET Electr. Power Appl., vol. 1, no. 4, p. 489, 2007.

[22] S. Murata, "Innovation by in-wheel-motor drive unit," Vehicle Syst. Dyn., vol. 50, no. 6, pp. 807–830, Jun. 2012.

[23] K. J. Binns and D. W. Shimmin, "Relationship between rated torque and size of permanent magnet machines," IEE Proc. Electr. Power Appl., vol. 143, no. 6, pp. 417–422, 1996.

[24] A. M. El-Refaie, "Fractional-slot concentrated-windings synchronous permanent magnet machines: Opportunities and challenges," IEEE Trans. Ind. Electron., vol. 57, no. 1, pp. 107–121, Jan. 2010.

[25] A. M. El-Refaie, M. R. Shah, R. Qu, and J. M. Kern, "Effect of number of phases on losses in conducting sleeves of surface PM machine rotors equipped with fractional-slot concentrated windings," IEEE Trans. Ind. Appl., vol. 44, no. 5, pp. 1522–1532, Sep. 2008.

[26] E. Fornasiero, N. Bianchi, and S. Bolognani, "Slot harmonic impact on rotor losses in fractional-slot permanent-magnet machines," IEEE Trans. Ind. Electron., vol. 59, no. 6, pp. 2557–2564, Jun. 2012.

[27] A. S. Abdel-Khalik, S. Ahmed, and A. M. Massoud, "Low space harmonics cancelation in double-layer fractional slot winding using dual multiphase winding," IEEE Trans. Magn., vol. 51, no. 5, pp. 1–10, May 2015.

[28] M. Nakano, H. Kometani, and M. Kawamura, "A study on eddy-current losses in rotors of surface permanent-magnet synchronous machines," IEEE Trans. Ind. Appl., vol. 42, no. 2, pp. 429–435, Mar. 2006.

[29] G. Dajaku, W. Xie, and D. Gerling, "Reduction of low space harmonics for the fractional slot concentrated windings using a novel stator design," IEEE Trans. Magn., vol. 50, no. 5, pp. 1–12, May 2014.

[30] J. Wang, X. Yuan, and K. Atallah, "Design optimization of a surface-mounted permanent-magnet motor with concentrated windings for electric vehicle applications," IEEE Trans. Veh. Technol., vol. 62, no. 3, pp. 1053–1064, Mar. 2013.

[31] E. Carraro, N. Bianchi, S. Zhang, and M. Koch, "Design and performance comparison of fractional slot concentrated winding spoke type synchronous motors with different slot-pole combinations," IEEE Trans. Ind. Appl., vol. 54, no. 3, pp. 2276–2284, May 2018.

[32] A. S. Abdel-Khalik, S. Ahmed, and A. M. Massoud, "A six-phase 24-Slot/10-Pole permanent-magnet machine with low space harmonics for electric vehicle applications," IEEE Trans. Magn., vol. 52, no. 6, pp. 1–10, Jun. 2016.

[33] K. Wang, Z. Q. Zhu, G. Ombach, M. Koch, S. Zhang, and J. Xu, "Electromagnetic performance of an 18-Slot/10-Pole fractional-slot surface-mounted permanent-magnet machine," IEEE Trans. Ind. Appl., vol. 50, no. 6, pp. 3685–3696, Nov. 2014.

[34] M. Kwon and S. Choi, "An electrolytic capacitorless bidirectional EV charger for V2G and V2H applications," IEEE Trans. Power Electron., vol. 32, no. 9, pp. 6792–6799, Sep. 2017.

[35] J. R. Pillai and B. Bak-Jensen, "Integration of vehicle-to-grid in the western Danish power system," IEEE Trans. Sustain. Energy, vol. 2, no. 1, pp. 12–19, Jan. 2010.

[36] A. Khaligh and S. Dusmez, "Comprehensive topological analysis of conductive and inductive charging solutions for plug-in electric vehicles," IEEE Trans. Veh. Technol., vol. 61, no. 8, pp. 3475–3489, Oct. 2012.

[37] I. Subotic, N. Bodo, and E. Levi, "Single-phase on-board integrated battery chargers for EVs based on multiphase machines," IEEE Trans. Power Electron., vol. 31, no. 9, pp. 6511–6523, Sep. 2016.

[38] I. Subotic, V. Katic, N. Bodo, E. Levi, B. Dumnic, and D. Milicevic, "Overview of fast on-board integrated battery chargers for electric vehicles based on multiphase machines and power electronics," IET Electr. Power Appl., vol. 10, no. 3, pp. 217–229, Mar. 2016.

[39] I. Subotic and E. Levi, "A review of single-phase on-board integrated battery charging topologies for electric vehicles," in Proc. IEEE Workshop Electr. Mach. Design, Control Diagnosis (WEMDCD), Mar. 2015, pp. 136–145.

[40] D. Thimmesch, "An SCR inverter with an integral battery charger for electric vehicles," IEEE Trans. Ind. Appl., vol. IA-21, no. 4, pp. 1023–1029, Jul. 1985.

[41] W. E. Rippel and A. G. Cocconi, "Integrated motor drive and recharge system," Google Patents 5 099 186, Mar. 24, 1992.

[42] L. Tang and G.-J. Su, "Control scheme optimization for a low-cost, digitally-controlled charger for plug-in hybrid electric vehicles," in Proc. IEEE Energy Convers. Congr. Exposit., Sep. 2010, pp. 3604–3610.

[43] A. G. Cocconi, "Combined motor drive and battery recharge system," Google Patents 5 341 075, 1994.

[44] S.-K. Sul and S.-J. Lee, "An integral battery charger for four-wheel drive electric vehicle," IEEE Trans. Ind. Appl., vol. 31, no. 5, pp. 1096–1099, Sep. 1995.

[45] L. Solero, "Nonconventional on-board charger for electric vehicle propulsion batteries," IEEE Trans. Veh. Technol., vol. 50, no. 1, pp. 144–149, Jan. 2001.

[46] G. Pellegrino, E. Armando, and P. Guglielmi, "An integral battery charger with power factor correction for electric scooter," IEEE Trans. Power Electron., vol. 25, no. 3, pp. 751–759, Mar. 2010.

[47] H.-C. Chang and C.-M. Liaw, "An integrated Driving/Charging switched reluctance motor drive using three-phase power module," IEEE Trans. Ind. Electron., vol. 58, no. 5, pp. 1763–1775, May 2011.

[48] T. J. E. Miller, Switched Reluctance Motors and Their Control. Oxford, U.K.: Clarendon, 1993.

[49] T. Na, X. Yuan, J. Tang, and Q. Z. Hang, "A review of on-board integrated electric vehicles charger and a new single-phase integrated charger," CPSS Trans. Power Electron. Appl., vol. 4, no. 4, pp. 288–298, Dec. 2019.

[50] I. Subotic, N. Bodo, E. Levi, and M. Jones, "Onboard integrated battery charger for EVs using an asymmetrical nine-phase machine," IEEE Trans. Ind. Electron., vol. 62, no. 5, pp. 3285–3295, May 2015.

[51] I. Subotic, N. Bodo, E. Levi, M. Jones, and V. Levi, "Isolated chargers for EVs incorporating six-phase machines," *IEEE Trans. Ind. Electron.*, vol. 63, no. 1, pp. 653–664, Jan. 2016.

[52] I. Subotic, N. Bodo, and E. Levi, "An EV drive-train with integrated fast charging capability," *IEEE Trans. Power Electron.*, vol. 31, no. 2, pp. 1461–1471, Feb. 2016.

[53] L. De Sousa, B. Silvestre, and B. Bouchez, "A combined multiphase electric drive and fast battery charger for electric vehicles," in *Proc. IEEE Vehicle Power Propuls. Conf.*, Sep. 2010, pp. 1–6.

[54] Y. Bai, X. Yang, D. Zhang, X. Li, W. Chen, and W. Hu, "Conducted EMI mitigation schemes in isolated switching-mode power supply without the need of a Y-Capacitor," *IEEE Trans. Power Electron.*, vol. 32, no. 4, pp. 2687–2703, Apr. 2017.

[55] A. Bruyere, L. De Sousa, B. Bouchez, P. Sandulescu, X. Kestelyn, and E. Semail, "A multiphase traction/fast-battery-charger drive for electric or plug-in hybrid vehicles: Solutions for control in traction mode," in *Proc. IEEE Vehicle Power Propuls. Conf.*, Sep. 2010, pp. 1–7.

[56] S. Lacroix, E. Laboure, and M. Hilairet, "An integrated fast battery charger for electric vehicle," in *Proc. IEEE Vehicle Power Propuls. Conf.*, Sep. 2010, pp. 1–6.

[57] A. P. Sandulescu, E. Semail, A. Bruyere, F. Meinguet, and X. Kestelyn, "Flux-weakening operation of open-end winding drive integrating a cost-effective high-power charger," *IET Electr. Syst. Transp.*, vol. 3, no. 1, pp. 10–21, Mar. 2013.

[58] S. Haghbin and O. Carlson, "Integrated motor drive and non-isolated battery charger based on the split-phase PM motors for plug-in vehicles," *J. Eng.*, vol. 2014, no. 6, pp. 275–283, Jun. 2014.

[59] S. Haghbin, S. Lundmark, M. Alakula, and O. Carlson, "An isolated high-power integrated charger in electrified-vehicle applications," *IEEE Trans. Veh. Technol.*, vol. 60, no. 9, pp. 4115–4126, Nov. 2011.

[60] A. S. Abdel-Khalik, M. S. Hamad, A. M. Massoud, and S. Ahmed, "Postfault operation of a nine-phase six-terminal induction machine under single open-line fault," *IEEE Trans. Ind. Electron.*, vol. 65, no. 2, pp. 1084–1096, Feb. 2018.

[61] A. S. Abdel-Khalik, S. Ahmed, and A. M. Massoud, "Performance evaluation of an on-board integrated battery charger system using a 12-slot/10-pole surface-mounted PM propulsion motor," presented at the 9th IEEE-GCC Conf. Exhib. (GCCCE), 2017.

[62] M. S. Diab, A. A. Elserougi, A. S. Abdel-Khalik, A. M. Massoud, and S. Ahmed, "A nine-switch-converter-based integrated motor drive and battery charger system for EVs using symmetrical six-phase machines," *IEEE Trans. Ind. Electron.*, vol. 63, no. 9, pp. 5326–5335, Sep. 2016.

[63] E. Levi, M. Jones, S. N. Vukosavic, and H. A. Toliyat, "A novel concept of a multiphase, multimotor vector controlled drive system supplied from a single voltage source inverter," *IEEE Trans. Power Electron.*, vol. 19, no. 2, pp. 320–335, Mar. 2004.

[64] I. Subotic, N. Bodo, and E. Levi, "Integration of six-phase EV drivetrains into battery charging process with direct grid connection," *IEEE Trans. Energy Convers.*, vol. 32, no. 3, pp. 1012–1022, Sep. 2017.

[65] K. A. Chinmaya and G. K. Singh, "Integrated onboard single-stage battery charger for PEVs incorporating asymmetrical six-phase induction machine," *IET Electr. Syst. Transp.*, vol. 9, no. 1, pp. 8–15, Mar. 2019.

[66] D. Herrera, J. Villegas, E. Galván, and J. M. Carrasco, "Synchronous reluctance six-phase motor proved based EV powertrain as charger/discharger with redundant topology and ORS control," *IET Electr. Power Appl.*, vol. 13, no. 11, pp. 1857–1870, Nov. 2019.

[67] C. Shi, Y. Tang, and A. Khaligh, "A three-phase integrated onboard charger for plug-in electric vehicles," *IEEE Trans. Power Electron.*, vol. 33, no. 6, pp. 4716–4725, Jun. 2018.

[68] C. Shi and A. Khaligh, "A two-stage three-phase integrated charger for electric vehicles with dual cascaded control strategy," *IEEE J. Emerg. Sel. Topics Power Electron.*, vol. 6, no. 2, pp. 898–909, Jun. 2018.

[69] C. Viana and P. W. Lehn, "A drivetrain integrated DC fast charger with buck and boost functionality and simultaneous drive/charge capability," *IEEE Trans. Transport. Electrific.*, vol. 5, no. 4, pp. 903–911, Dec. 2019.

[70] V. F. Pires, J. Monteiro, A. Cordeiro, and J. F. Silva, "Integrated battery charger for electric vehicles based on a dual-inverter drive and a three-phase current rectifier," *Electronics*, vol. 8, no. 10, p. 1199, 2019.

[71] A. Iqbal, S. Moinuddin, M. R. Khan, S. M. Ahmed, and H. Abu-Rub, "A novel three-phase to five-phase transformation using a special transformer connection," *IEEE Trans. Power Del.*, vol. 25, no. 3, pp. 1637–1644, Jul. 2010.

[72] S. Moinoddin, A. Iqbal, H. Abu-Rub, M. R. Khan, and S. M. Ahmed, "Three-phase to seven-phase power converting transformer," *IEEE Trans. Energy Convers.*, vol. 27, no. 3, pp. 757–766, Sep. 2012.

[73] S. M. Ahmed, A. Iqbal, and H. Abu-Rub, "Generalized duty-ratio-based pulsewidth modulation technique for a three-to-*k* phase matrix converter," *IEEE Trans. Ind. Electron.*, vol. 58, no. 9, pp. 3925–3937, Sep. 2011.

[74] A. Iqbal, H. Abu-Rub, J. Rodriguez, C. A. Rojas, and M. Saleh, "Simple carrier-based PWM technique for a three-to-nine-phase direct AC–AC converter," *IEEE Trans. Ind. Electron.*, vol. 58, no. 11, pp. 5014–5023, Nov. 2011.

[75] I. Subotic, E. Levi, M. Jones, and D. Graovac, "An integrated battery charger for EVs based on an asymmetrical six-phase machine," in *Proc. 39th Annu. Conf. IEEE Ind. Electron. Soc. (IECON)*, Nov. 2013, pp. 7244–7249.

[76] I. Subotic, E. Levi, M. Jones, and D. Graovac, "Multiphase integrated on-board battery chargers for electrical vehicles," in *Proc. 15th Eur. Conf. Power Electron. Appl. (EPE)*, Sep. 2013, pp. 1–10.

[77] I. Subotic and E. Levi, "An integrated battery charger for EVs based on a symmetrical six-phase machine," in *Proc. IEEE 23rd Int. Symp. Ind. Electron. (ISIE)*, Jun. 2014, pp. 2074–2079.

[78] S. Dusmez, A. Cook, and A. Khaligh, "Comprehensive analysis of high quality power converters for level 3 off-board chargers," in *Proc. IEEE Vehicle Power Propuls. Conf.*, Sep. 2011, pp. 1–10.

[79] J. Dannehl, C. Wessels, and F. W. Fuchs, "Limitations of voltage-oriented PI current control of grid-connected PWM rectifiers with *LCL* filters," *IEEE Trans. Ind. Electron.*, vol. 56, no. 2, pp. 380–388, Feb. 2009.

[80] A. T. Al-Awami, E. Sortomme, G. M. A. Akhtar, and S. Faddel, "A voltage-based controller for an electric-vehicle charger," *IEEE Trans. Veh. Technol.*, vol. 65, no. 6, pp. 4185–4196, Jun. 2016.

[81] A. S. Abdel-Khalik, S. Ahmed, and A. Massoud, "A bearingless coaxial magnetic gearbox," *Alexandria Eng. J.*, vol. 53, no. 3, pp. 573–582, Sep. 2014.

[82] A. S. Abdel-Khalik and S. Ahmed, "Performance evaluation of a five-phase modular external rotor PM machine with different rotor poles," *Alexandria Eng. J.*, vol. 51, no. 4, pp. 249–261, Dec. 2012.

[83] A. S. Abdel-Khalik, "Five-phase modular external rotor PM machines with different rotor poles: A comparative simulation study," *Model. Simul. Eng.*, vol. 2012, pp. 1–14, Sep. 2012.

[84] V. I. Patel, J. Wang, W. Wang, and X. Chen, "Six-phase fractional-slot-per-pole-per-phase permanent-magnet machines with low space harmonics for electric vehicle application," *IEEE Trans. Ind. Appl.*, vol. 50, no. 4, pp. 2554–2563, Jul. 2014.

[85] J. Cros and P. Viarouge, "Synthesis of high performance PM motors with concentrated windings," *IEEE Trans. Energy Convers.*, vol. 17, no. 2, pp. 248–253, Jun. 2002.

[86] D. A. Stone, P. H. Mellor, D. Howe, and K. Atallah, "Rotor loss in permanent-magnet brushless AC machines," *IEEE Trans. Ind. Appl.*, vol. 36, no. 6, pp. 1612–1618, Nov. 2000.

[87] N. Bianchi and E. Fornasiero, "Index of rotor losses in three-phase fractional-slot permanent magnet machines," *IET Electr. Power Appl.*, vol. 3, no. 5, pp. 381–388, 2009.

[88] M. R. Shah and S. Bin Lee, "Rapid analytical optimization of eddy-current shield thickness for associated loss minimization in electrical machines," *IEEE Trans. Ind. Appl.*, vol. 42, no. 3, pp. 642–649, May 2006.

[89] A. S. Abdel-Khalik, S. Ahmed, and A. Massoud, "Application of stator shifting to five-phase fractional-slot concentrated winding interior permanent magnet synchronous machine," *IET Electr. Power Appl.*, vol. 10, no. 7, pp. 681–690, Aug. 2016.

[90] P. B. Reddy, K.-K. Huh, and A. M. El-Refaie, "Generalized approach of stator shifting in interior permanent-magnet machines equipped with fractional-slot concentrated windings," *IEEE Trans. Ind. Electron.*, vol. 61, no. 9, pp. 5035–5046, Sep. 2014.

[91] F. Libert and J. Soulard, "Investigation on pole-slot combinations for permanent-magnet machines with concentrated windings," in *Proc. ICEM*, 2004, pp. 530–535.

[92] A. M. El-Refaie and T. M. Jahns, "Optimal flux weakening in surface PM machines using fractional-slot concentrated windings," *IEEE Trans. Ind. Appl.*, vol. 41, no. 3, pp. 790–800, May 2005.

[93] F. Magnussen and C. Sadarangani, "Winding factors and joule losses of permanent magnet machines with concentrated windings," in *Proc. IEEE Int. Electr. Mach. Drives Conf. (IEMDC)*, vol. 1, Jun. 2003, pp. 333–339.

[94] F. Meier, "Permanent-magnet synchronous machines with non-overlapping concentrated windings for low-speed direct-drive applications," Ph.D. dissertation, Dept. Elect. Eng., KTH, Stockholm, Sweden, 2008.

[95] P. B. Reddy, A. M. El-Refaie, and K.-K. Huh, "Effect of number of layers on performance of fractional-slot concentrated-windings interior permanent magnet machines," *IEEE Trans. Power Electron.*, vol. 30, no. 4, pp. 2205–2218, Apr. 2015.

[96] N. Bianchi and M. Dai Pre, "Use of the star of slots in designing fractional-slot single-layer synchronous motors," *IEE Proc. Electr. Power Appl.*, vol. 153, no. 3, pp. 459–466, 2006.

[97] Y. Zhang, "A novel 24-slots14-poles fractional-slot concentrated winding topology with low space harmonics for electrical machines," *Energies*, vol. 11, no. 5, pp. 1–6, 2018.

[98] N. Bianchi, S. Bolognani, M. D. Pre, and G. Grezzani, "Design considerations for fractional-slot winding configurations of synchronous machines," *IEEE Trans. Ind. Appl.*, vol. 42, no. 4, pp. 997–1006, Jul. 2006.

[99] G. Dajaku and D. Gerling, "A novel 24-slots/10-poles winding topology for electric machines," in *Proc. IEEE Int. Electr. Mach. Drives Conf. (IEMDC)*, May 2011, pp. 65–70.

[100] P. Zheng, F. Wu, Y. Lei, Y. Sui, and B. Yu, "Investigation of a novel 24-slot/14-pole six-phase fault-tolerant modular permanent-magnet in-wheel motor for electric vehicles," *Energies*, vol. 6, no. 10, pp. 4980–5002, 2013.

[101] Z. Q. Zhu, M. L. Mohd Jamil, and L. J. Wu, "Influence of slot and pole number combinations on unbalanced magnetic force in PM machines with diametrically asymmetric windings," *IEEE Trans. Ind. Appl.*, vol. 49, no. 1, pp. 19–30, Jan. 2013.

[102] M. Barcaro, N. Bianchi, and F. Magnussen, "Six-phase supply feasibility using a PM fractional-slot dual winding machine," in *Proc. IEEE Energy Convers. Congr. Exposit.*, Sep. 2010, pp. 1058–1065.

[103] M. Barcaro, N. Bianchi, and F. Magnussen, "Six-phase supply feasibility using a PM fractional-slot dual winding machine," *IEEE Trans. Ind. Appl.*, vol. 47, no. 5, pp. 2042–2050, Sep. 2011.

[104] H. Dhulipati, E. Ghosh, S. Mukundan, P. Korta, J. Tjong, and N. C. Kar, "Advanced design optimization technique for torque profile improvement in six-phase PMSM using supervised machine learning for direct-drive EV," *IEEE Trans. Energy Convers.*, vol. 34, no. 4, pp. 2041–2051, Dec. 2019.

[105] Z. Q. Zhu, D. Wu, and X. Ge, "Investigation of voltage distortion in fractional slot interior permanent magnet machines having different slot and pole number combinations," *IEEE Trans. Energy Convers.*, vol. 31, no. 3, pp. 1192–1201, Sep. 2016.

[106] V. I. Patel, J. Wang, D. T. Nugraha, R. Vuletic, and J. Tousen, "Enhanced availability of drivetrain through novel multiphase permanent-magnet machine drive," *IEEE Trans. Ind. Electron.*, vol. 63, no. 1, pp. 469–480, Jan. 2016.

[107] H. V. Xuan, D. Lahaye, H. Polinder, and J. A. Ferreira, "Influence of slot/pole number combination on performances of permanent magnet machines with concentrated windings for ship application," in *Proc. Int. Conf. Electr. Mach. Syst.*, Aug. 2011, pp. 1–6.

[108] H. Dhulipati, S. Mukundan, W. Li, J. Tjong, and N. C. Kar, "Investigation of phase angle displacements in six-phase PMSM with concentrated windings for reduced MMF harmonics," in *Proc. 21st Int. Conf. Electr. Mach. Syst. (ICEMS)*, Oct. 2018, pp. 308–313.

[109] Y. Wang, R. Qu, and J. Li, "Multilayer windings effect on interior PM machines for EV applications," *IEEE Trans. Ind. Appl.*, vol. 51, no. 3, pp. 2208–2215, May 2015.

[110] A. Khaligh and M. D'Antonio, "Global trends in high-power on-board chargers for electric vehicles," *IEEE Trans. Veh. Technol.*, vol. 68, no. 4, pp. 3306–3324, Apr. 2019.

[111] M. Y. Metwly, M. S. Abdel-Majeed, A. S. Abdel-Khalik, M. Torki, R. A. Hamdy, M. S. Hamad, and S. Ahmed, "IoT-based supervisory control of an asymmetrical nine-phase integrated on-board EV battery charger," *IEEE Access*, vol. 8, pp. 62619–62631, 2020.

[112] N. Bodo, E. Levi, I. Subotic, J. Espina, L. Empringham, and C. M. Johnson, "Efficiency evaluation of fully integrated on-board EV battery chargers with nine-phase machines," *IEEE Trans. Energy Convers.*, vol. 32, no. 1, pp. 257–266, Mar. 2017.

MOHAMED Y. METWLY received the B.Sc. degree in electrical engineering from Alexandria University, Alexandria, Egypt, in 2018. He is currently a Researcher with Smart-CI, Alexandria University. His current research interests include battery chargers, electric vehicles, and renewable energy systems.

MAHMOUD S. ABDEL-MAJEED received the B.Sc. degree in electrical engineering from Alexandria University, Alexandria, Egypt, in 2019. He is currently a Researcher with Smart-CI, Alexandria University. His current research interests include battery chargers, automotive, smart grid, and power electronics.

AYMAN S. ABDEL-KHALIK (Senior Member, IEEE) received the B.Sc. and M.Sc. degrees in electrical engineering from Alexandria University, Alexandria, Egypt, in 2001 and 2004, respectively, and the Ph.D. degree in electrical engineering from Alexandria University and Strathclyde University, Glasgow, U.K., in 2009, under a Dual Channel Program. He is currently a Professor with the Department of Electrical Engineering, Faculty of Engineering, Alexandria University. His current research interests include electrical machine design and modeling, electric drives, energy conversion, and renewable energy. He serves as an Associate Editor for the IEEE Transactions on Industrial Electronics and the *IET Electric Power Applications* Journal. He also serves as the Executive Editor of the *Alexandria Engineering Journal*.

RAGI A. HAMDY (Senior Member, IEEE) received the B.Sc. and M.Sc. degrees from Alexandria University, Alexandria, Egypt, in 1991 and 1994, respectively, and the Ph.D. degree from Heriot-Watt University, U.K., in 1999. He is currently a Professor with the Department of Electrical Engineering, Faculty of Engineering, Alexandria University. His current research interests include electric machines, electric drives, and power electronics.

MOSTAFA S. HAMAD (Senior Member, IEEE) received the B.Sc. and M.Sc. degrees in electrical engineering from Alexandria University, Alexandria, Egypt, in 1999 and 2003, respectively, and the Ph.D. degree in electrical engineering from Strathclyde University, Glasgow, U.K., in 2009.

From 2010 to 2014, he was an Assistant Professor with the Department of Electrical and Control Engineering, College of Engineering and Technology, Arab Academy for Science, Technology and Maritime Transport (AASTMT), Alexandria, where he is currently a Professor. His research interests include power electronics applications in power quality, electric drives, distributed generation, HVDC transmission systems, and renewable energy.

SHEHAB AHMED (Senior Member, IEEE) received the B.Sc. degree in electrical engineering from Alexandria University, Alexandria, Egypt, in 1999, and the M.Sc. and Ph.D. degrees from the Department of Electrical and Computer Engineering, Texas A&M University, College Station, TX, USA, in 2000 and 2007, respectively. He was with Schlumberger Technology Corporation, Houston, TX, USA, from 2001 to 2007, developing downhole mechatronic systems for oilfield service products. He was with Texas A&M University at Qatar from 2007 to 2018. He joined the King Abdullah University of Science and Technology (KAUST), Saudi Arabia, in 2018, where he is currently a Professor of electrical engineering with the CEMSE Division. His research interests include mechatronics, solid-state power conversion, and electric machines.

. . .